249

SAND80-1138
Unlimited Release
UC-13

In-Situ Stress From Hydraulic Fracture Measurements in G Tunnel, Nevada Test Site

Carl Smith, William C. Vollendorf, William E. Warren

Sandia National Laboratories

SF 2900-Q(3-80)

Issued by Sandia National Laboratories, operated for the United States Department of Energy by Sandia Corporation.

NOTICE: This report was prepared as an account of work sponsored by an agency of the United States Government. Neither the United States Government nor any agency thereof, nor any of their employees, nor any of their contractors, subcontractors, or their employees, makes any warranty, express or implied, or assumes any legal liability or responsibility for the accuracy, completeness, or usefulness of any information, apparatus, product, or process disclosed, or represents that its use would not infringe privately owned rights. Reference herein to any specific commercial product, process, or service by trade name, trademark, manufacturer, or otherwise, does not necessarily constitute or imply its endorsement, recommendation, or favoring by the United States Government, any agency thereof or any of their contractors or subcontractors. The views and opinions expressed herein do not necessarily state or reflect those of the United States Government, any agency thereof or any of their contractors or subcontractors.

Printed in the United States of America

Available from
National Technical Information Service
U. S. Department of Commerce
5285 Port Royal Road
Springfield, VA 22161

NTIS price codes
Printed copy: $7.00
Microfiche copy: A01

SAND80-1138
Unlimited Release
Printed April 1981

Distribution
Category UC-13

IN-SITU STRESS FROM HYDRAULIC FRACTURE MEASUREMENTS IN G TUNNEL, NEVADA TEST SITE

Carl Smith
Experiments Planning Division 1112

William C. Vollendorf
Engineering Projects Division 1133

William E. Warren
Computational Physics and
Mechanical Division I

Sandia National Laboratories
Albuquerque, NM 87185

ABSTRACT

This report discusses hydraulic fracture work in G Tunnel, Nevada Test Site, performed to obtain the in-situ stress state. Field equipment and procedures are described; analysis is developed to relate the hydraulic fracture pressures to the in-situ stress state. Pressure data are analyzed to provide estimates of the stress state at a number of locations in the tunnel complex. A unique feature of the work is the mineback--a mining process in which the rock is cut away to reveal the actual plane of the fracture. Advantages, limitations, and problem areas associated with extracting in-situ stress fields from hydraulic fracture pressure records are discussed in detail.

CONTENTS

	Page
Introduction	9
Background	10
Hydraulic Fracture and In-Situ Stress	10
Geologic Setting	13
Equipment and Field Techniques	14
Selective Data	16
Data from HFS 7, 8, and 9 (1974)	16
Data from HFS 10, 11, and 12 (1974)	19
Data from HF 20 (1977), HF 39, 40 (1978)	20
Data from HF 45 and 46 (1978)	20
Stress Analysis	23
Stresses at a Horizontal Borehole with One Principal Stress Vertical	25
Results	30
Analysis of HFS 7, 8, and 9	30
Analysis of HFS 10, 11, and 12	32
Analysis of HF 20, 39, and 40	34
Analysis of HF 45 and 46	35
Summary	41
References	48
APPENDIX A -- Hydrofrac Hole List (U12G)	51
APPENDIX B -- Complete Stress and Displacement Fields	53
APPENDIX C -- Uniform Stress Field Referred to Principal Stresses	61
APPENDIX D -- Overburden Stress under an Inclined Geologic Surface	65

ILLUSTRATIONS

Figure		
Frontispiece	-- The Alpine Miner	7
1	Geometry of Vertical Drill Hole Aligned Parallel to Principal Stress	11
2	Classical Hydrofrac Fracturing Pressure-Time and Flow-Time Charts	12
3	Hydrofrac Pumping System	15
4	Mineback Procedure for HF 46 Fracture	21
5	Top Views of Turning Fracture Observed on HF 46 Mineback	22
6	Geometry of Borehole with One Principal Stress Normal	26
7	Plot of σ_{min} versus Position θ around Borehole for Several Angles α	28
8	Critical Pressure P_c versus Borehole Orientation Angle α	29

ILLUSTRATIONS (Continued)

Figure		Page
9	Orientation of Fracture Plane and Principal Stresses, HFS 7, 8, and 9	31
10	Orientation of Fracture Plane and Principal Stresses, HFS 10, 11, and 12	34
11	Orientation of Fracture Plane and Principal Stresses, HF 20, 39, and 40	36
12	Pressure-Time Record for HF 46, Zone R8 -- 22 Feet	37
13	Vertical Section through G Tunnel, Showing Direction of Induced Fractures	43
14	G Tunnel Map, Showing Azimuths of Induced Fractures	44

TABLES

Table		
1	Hydrofracture Data	17
2	12g Tuff Physical Properties Laboratory Tests	18
3	Angle of Minimum Stress γ with Distance r/R_o from the Borehole	40
4	Overcore and Hydrofrac Tests Compared	41

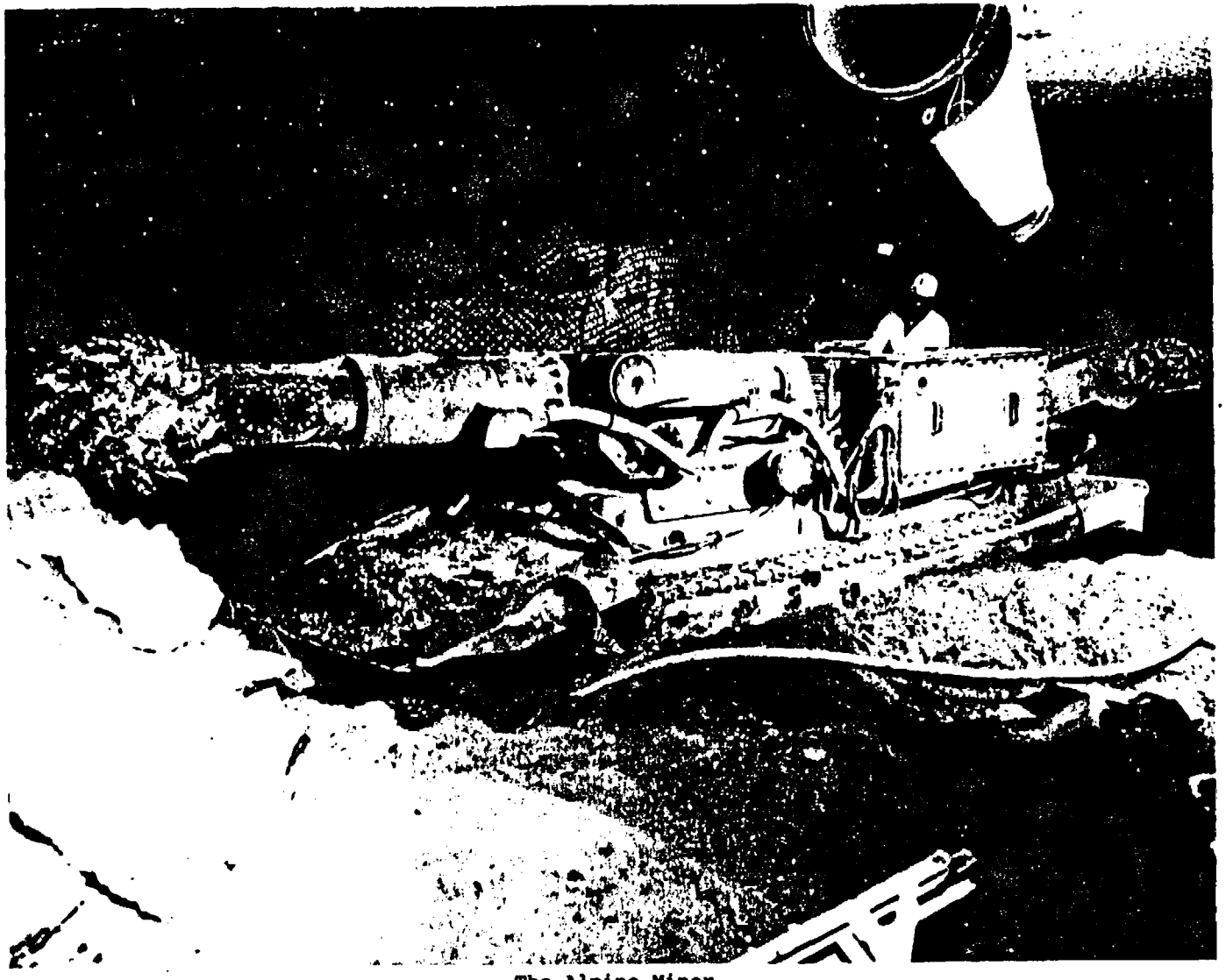

The Alpine Miner

FRONTISPIECE

IN-SITU STRESS FROM HYDRAULIC FRACTURE MEASUREMENTS IN G TUNNEL, NEVADA TEST SITE

Introduction

This report discusses estimates of in-situ stresses in G Tunnel, Rainier Mesa, Nevada Test Site (NTS), obtained with hydraulic fracture (hydrofrac) techniques. This stress state is related to containment of underground nuclear detonations. Gases that escape from a cavity formed by a nuclear explosion will pressurize accessible drifts and, with sufficient amplitude, will fracture the surrounding rock. An example is the radioactive fracture that was caused in the DEEP WELL drift by the pressure from escaped gases of the decoupled RED HOT event. Knowledge of in-situ stresses will allow prediction of both the direction of these fractures and the approximate value of the pressures necessary to drive the fractures. In-situ stress data may also be useful for siting future nuclear events. If, for example, a zone of anomalous stress was encountered, the site probably would be avoided unless the source of the anomaly was understood.

Hydrofrac work in G Tunnel began in 1974; the early results have been summarized.[1] Since then, equipment has been improved, and better techniques of analysis have been developed. This report includes descriptions of this improved equipment, field procedures used, techniques of analysis, and definition of several problem areas encountered during the course of the work. Estimates are provided of the stress state at several locations in the tunnel complex. First, the background on hydrofrac techniques is summarized, and the geologic setting is presented. Then, details of the equipment, the operating procedures, and the process of uncovering the fractures (mineback) are given. The mineback process is unique in that it allows tracing of the fracture plane away from the hydrofrac hole and investigation of its behavior. A series of selected hydrofrac operations is described, and the data obtained are presented. Next, the determination of in-situ stresses by analyzing hydrofrac measurements is explained. Limitations and problem areas are discussed. Then, analysis is applied to selected hydrofrac data. Finally, a summary section includes a map of in-situ stresses in G Tunnel, a discussion of how these stresses relate to the surrounding topography, a comparison of stresses obtained with hydrofrac techniques with those obtained with overcore techniques, and a discussion of general problems encountered when determining in-situ stresses from hydrofrac data.

For record purposes, Appendix A provides a tabulation of G-Tunnel hydrofrac holes and their status. Appendix B contains the derivation of the complete stress and displacement fields in an unbounded elastic media containing an infinitely-long pressurized cylindrical cavity with a general stress state at infinity. In Appendix C, these stresses at infinity are related to the principal stresses through Euler's angles. Appendix D analyzes overburden stresses under an inclined terrain.

Background

Hydraulic Fracture and In-Situ Stress

For many years, the process of hydraulic fracturing has been used to enhance recovery from oil and gas wells.[2] In general, the process provides flow paths in the oil- or gas-bearing geologic formation by creating a fracture of large extent in the formation. In practice, a section of the well is sealed off by packers and pressurized with a fluid until fracture of the borehole occurs. Continued pumping of the fluid after fracture drives the single fracture plane out into the formation, the fracture plane orienting itself normal to the minimum principal in-situ stress. A propping agent such as sand is often added to the fracture fluid to keep the crack faces separated after pumping has stopped and oil and gas recovery is resumed.

In 1957, Hubert and Willis[3] recognized that, under certain conditions, the magnitude of some components of the in-situ stress field could be estimated from pumping pressure records obtained during the hydrofrac operation. This idea has been pursued by several other researchers, including Scheidegger,[4] Kehle,[5] and Fairhurst,[6] who describe the advantages of this procedure relative to other established techniques. Basically, the hydrofrac technique offers the unique possibility of directly measuring both the magnitude and the direction of the minimum principal stress. Haimson performed extensive laboratory experiments that he described in his thesis.[7] An overview of the subject has been given by Haimson and Fairhurst.[8]

The classical hydrofrac operation involves fracturing a vertical borehole at a point sufficiently deep into the formation so that the overburden or vertical stress can be considered a principal stress parallel to the borehole and greater in magnitude than at least one of the horizontal principal stresses. Under these conditions, the fracture plane is vertical and normal to the minimum principal stress. The borehole lies in the fracture plane and the stress analysis for this classical situation is elementary. A fracture begins at the wall of a drill hole when fluid pressure exceeds the in-situ stress loading in the hole added to the tensile strength of the rock. The fracture propagates parallel to the axis of the hole when the axis is perpendicular to the minimum principal stress (Figure 1). For isotropic rock with low permeability and negligible pore pressure, the breakdown pressure (P_c) is related to the two principal stresses (σ_{max} and σ_{min}) by

$$P_c = 3\sigma_{min} - \sigma_{max} + T \qquad (1)$$

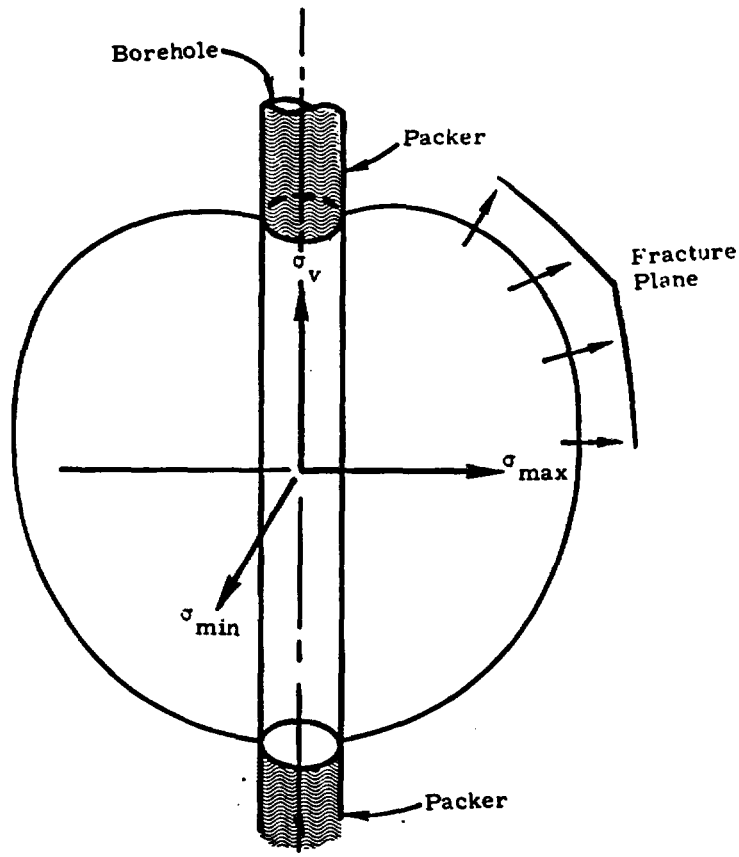

Figure 1. Geometry of Vertical Drill Hole Aligned Parallel to Principal Stress

where compressive stresses are positive and T is the tensile strength of the rock. The minimum principal stress is obtained from the pumping record in the following manner: If the borehole-fracturing fluid system is isolated ("shut in") at the moment the pump is turned off, the equilibrium pressure in the system is equal to the stress that loads the fracture. Since the fracture opens against the smallest of the in-situ stresses, this shut-in pressure (P_{si}) is assumed to be the minimum in-situ stress. Knowing the value of the tensile strength of the rock, two of the three principal in-situ stresses can thus be obtained. If the ground surface is relatively level, if the geology consists of horizontal beds, and if there is little horizontal tectonic stress, then one principal stress is vertical and the other two principal stresses are in the horizontal plane. Fractures will then be vertical in the plane of the borehole and propagate in the direction of the maximum horizontal stress and perpendicular to the minimum stress. The classic hydrofrac pressure record is shown in Figure 2. The shut-in pressure is equal to the minimum in-situ stress, and the maximum horizontal stress is calculated with Eq. (1). The third principal stress, the vertical or overburden stress, is usually estimated by considering the density and thickness of the rock above the packed-off interval.

This elementary analysis for vertical holes has been used extensively to estimate in-situ stress. A fault system in the Rangley oil field has been examined,[9,10] as have been stresses along a line perpendicular to the San Andreas

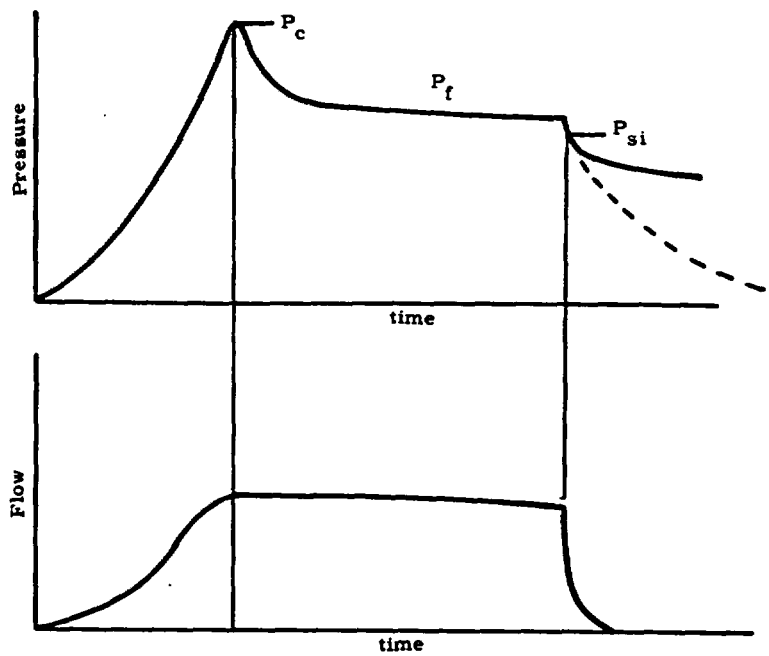

Figure 2. Classical Hydrofrac Fracturing Pressure-Time and Flow-Time Charts

fault.[11] In general, the results correspond with other indicators and with measurements of in-situ stress obtained, for example, from earthquake-fault mechanisms and overcoring techniques. Recently, Terra Tek, Inc., has attempted to analyze hydraulic fractures by using a fracture-mechanics approach.[12] The oil and gas industries have vigorously pursued the hydrofrac technique as a stimulation tool, and extensive literature exists on their efforts.[13] Los Alamos National Scientific Laboratory has used the technique to induce a fracture in deeply buried granite for its hot dry rock geothermal energy experiments.[14]

In some situations, none of the principal stresses may be vertical. This may happen, for example, if the ground surface is not level. Also, if one uses horizontal drill holes, they may not be parallel to a stress component. In such cases, more analysis is needed to calculate in-situ stresses from the hydrofrac measurements. This analysis is provided in "Stress Analysis" and in the Appendices B and C.

Hydrofrac techniques have been used previously to obtain in-situ stress values at Rainier Mesa. In N, E, and T Tunnels, the United States Geological Survey (USGS) performed a series of hydrofracs whose results agreed well with results obtained using overcoring techniques.[15] No stress directions were obtained. B. C. Haimson and Terra Tek, Inc.,[16] performed a series of hydrofracs in N-Tunnel and in a hole extending from the mesa surface downward almost to the N-Tunnel level. Extracted in-situ stress showed an increase with depth, as expected. At the level of the tunnel, the stresses were

- Vertical 70 bars (1015 lb/in^2)
- Horizontal maximum 88 bars (1276 lb/in^2)
- Horizontal minimum 35 bars (508 lb/in^2) ,

where the vertical stress was calculated from the overburden density and the depth. An impression packer showed the fractures to be vertical and aligned N35°E--the direction of the horizontal maximum stress. These values agree well with earlier, in-tunnel, Bureau of Mines overcoring.[17] An example of an in-situ stress state where no component is vertical is seen from the overcoring results from E Tunnel.[18] While the minimum principal stress is essentially horizontal, indicating a vertical fracture plane, the other two principal stresses are 50° and 40° from the vertical. If a vertical principal stress had been assumed and the classical hydrofrac analysis of Eq. (1) used, the results would be in considerable error.

The first Sandia work in G Tunnel has been described by Tyler and Vollendorf.[1] One hole was drilled vertically from the top of the mesa, and 15 holes were drilled horizontally and vertically from drifts in the tunnel complex. Fractures in two horizontal holes and at the bottom of the vertical hole from the mesa were examined with a mineback technique described later in this report. At tunnel level and under the cap of the mesa, vertical fractures were observed, and the following stresses* were obtained from pressure measurement in the vertical hole.

- Maximum horizontal 123 bars (1788 lb/in^2)
- Minimum horizontal 70 bars (1015 lb/in^2)
- Vertical 82 bars (1183 lb/in^2)

The azimuth of the maximum horizontal stress was N50°E. Fracture planes under the sloping portion of the mesa deviated from vertical, and hydrofrac-determined stress levels were less than those under the flat mesa cap.

Geologic Setting

Rainier Mesa consists of an approximately 1500-foot-thick series of thin-to-massive, bedded calc-alkaline and peralkaline ash-fall tuff, reworked tuff, and tuffaceous sandstone, capped by a massive welded ash-flow tuff unit. These tuff units unconformably overlie massive Paleozoic and older rocks.

The rock in which the hydrofrac tests were conducted consists of medium-to-massive bedded ash-fall tuff with occasional thin beds of peralkaline and reworked tuff. The bedded tuff units are light to reddish brown, fine- to medium-grained calc-alkaline tuff, with reworked tuffaceous sandstone beds in some places. The beds are generally zeolitized. The beds dip generally ~10° to the west, although local variations of 0° to ~25° exist. A normal fault with ~10-foot displacement occurs approximately 200 feet from HF 20 and the overcore area. Also, a depositional synclinal structure is located between the hydrofrac hole HF 20 and holes HFS 13, 14, and 15.

Typical physical properties of the tuff in which the experiments were conducted are

- Specific Gravity - 1.95
- Porosity - 33%

*Later in this report, slightly different values are shown for the stresses at this location because additional data were used.

- Water saturation - 97%
- Permeability - 0.1 mD
- Compressive strength - 3500 lb/in^2
- Tensile strength - 150 lb/in^2
- Poisson's ratio - 0.25
- Compressional sonic velocity - 8300 ft/s
- Shear velocity - 4500 ft/s

Equipment and Field Techniques

For hydrofracturing in the tunnel complex, a pumping system employing dual-action, air-driven Haskell pumps (Figure 3) is used. This system was first used for HF20; previous hydrofracs were performed with a system described in Reference 1. Two pumps will deliver up to 10 gal/min at pressures up to 2500 lb/in^2. If pressures exceed this level, another pump, capable of 5000 lb/in^2 but with a smaller flow rate, "kicks" in. The compartment tank, shown at the left end, holds 300 gallons of water to which various colored dyes are added to "mark" the fracture. A blue dye obtained from American Cyanamid Chemical Co. is the most successful because it remains in the fracture and is readily observed in the red-to-yellow tuff rock. A piston-type, positive-displacement meter measures flow at the input to the pump, and a turbine-type meter measures flow at the collar of the hole.

Pumping pressure is measured at the collar of the hole and, recently, also at the packer assembly. No hydrostatic head is involved because work is usually done in nearly-horizontal holes, 50 to 200 feet long. Similar pressures are recorded from both transducer locations for the usual quasi-static load conditions. Transient pressures, however, such as those occurring at breakdown, are recorded in sharper detail from the transducer located in the packer assembly.

The full-straddle packer assembly consists of two Lynes packers, Model 300.01; these packers are 66 inches long and designed for 4-inch-diameter holes. The packer assembly is the long cylindrical object in front of the pumping system (Figure 3); the complete assembly is 16 feet long. Spacing between the packers is controlled by a pipe; currently, the straddled length is 59 inches. Fluid passes through the packer nearest the hole collar and out through holes in the spacing pipe. The assembly is inserted into the hole on AQ drill pipe. A single packer is sometimes used when pressurizing the end of a hole.

Taped to the pipe is an electrical cable for the pressure transducer and a small-diameter hose which carries water to inflate and pressurize the packers. After the packer assembly has been inserted to the desired position, the packers are pumped to the desired pressure; a pressure which is about equal to the expected breakdown pressure.*

---

*On mineback, fractures were observed in the vicinity of the packers, suggesting that the packers themselves may have fractured the rock. A recent analysis by Warren[20] supports this possibility.

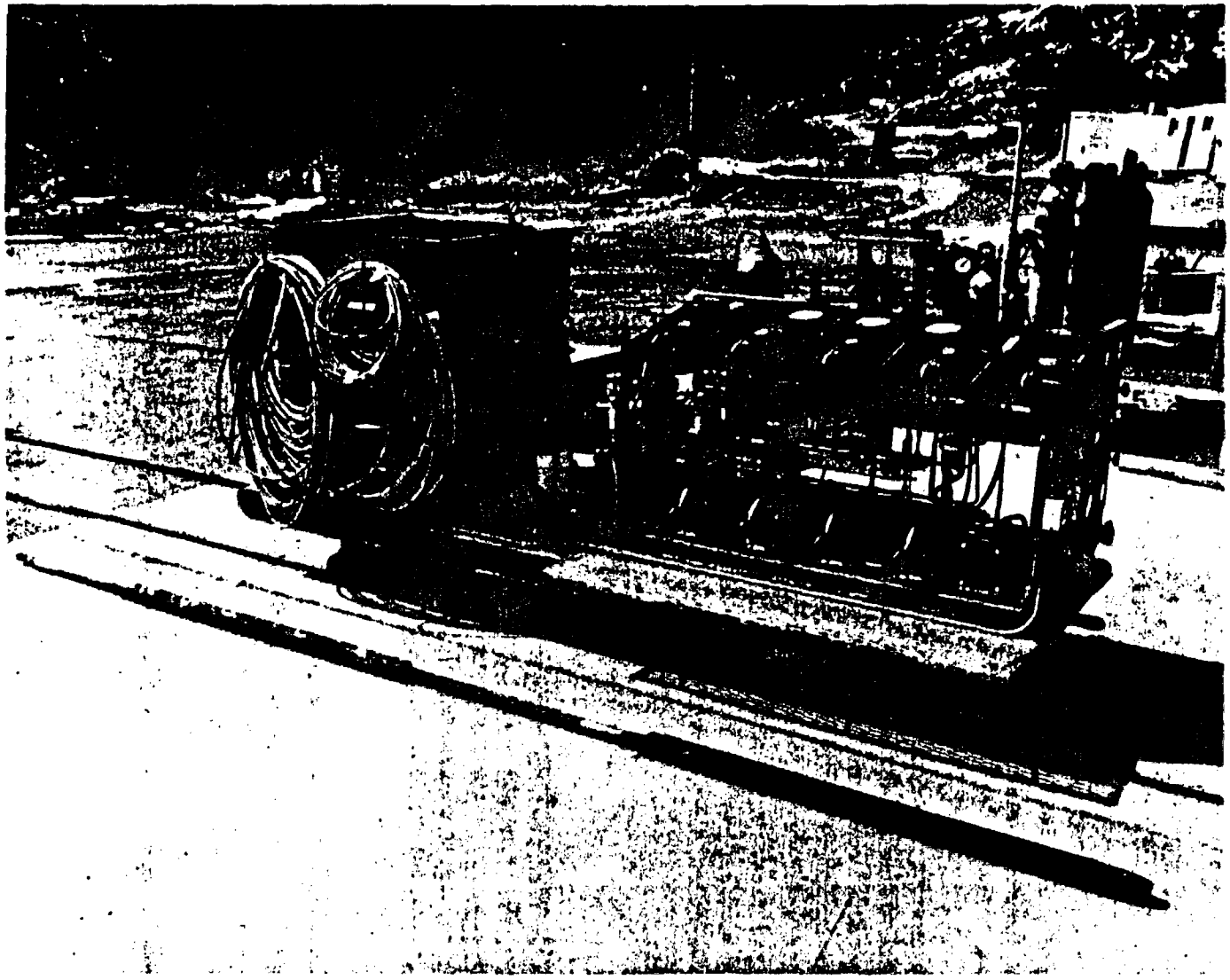

Figure 3. Hydrofrac Pumping System

Pumping is initiated, and the flow rate, usually 5 gal/min, is held constant. The pumping rate and pressure are recorded on a tape recorder and on an oscillograph. The oscillograph allows immediate access to the data, and the tape recording allows later processing of the data. After breakdown (P_c, Figure 2), we pump 5 to 10 gallons of fracture fluid and observe the fracture-driving pressure (P_f). A quarter-turn valve is used to isolate (shut-in) the pumping system from the fracture system; the shut-in pressure (P_{si}) in the fracture system is assumed to be the pressure needed to hold the fracture open and is of fundamental interest because it relates directly to the minimum in-situ stress. Figure 2 shows the classic behavior of P_{si}. Often, however, the pressure does not follow classic behavior but decays rapidly and does not show an inflection point on the curve. This behavior requires a judgment selection of the P_{si} point and contributes to uncertainties in P_{si}.

More than 50 fractures have been examined with a "mineback" process which utilizes the Alpine Miner, a continuous mining machine with a rotary head that "chews" the soft rock. This type of mineback allows a nearly continuous examination of the fractures and other features. The normal procedure is to mine a horizontal drift about 10 feet wide and 10 feet high, keeping the fractured hole at the center of the face. Approximately 1 to 2 feet at a time is mined; fractures on the face and other features are mapped in detail and photographed. Subsequently, face, plan, and vertical section maps are drawn from the field maps and photographs.

Selective Data

This section presents data obtained from selected hydrofractured boreholes in G Tunnel. These selected data are typical of all hydrofrac operations conducted to date. Field observations are described, and Table 1 summarizes the pressure magnitudes necessary to determine the in-situ stresses. Physical properties of the ash-fall tuff for regions of G Tunnel near the selected data points are listed, where available, in Table 2.

Data from HFS 7, 8, and 9 (1974)

HFS 7, 8, and 9 were an approximately orthogonal array of holes, 100 feet deep, located near Construction Station (CS) 8 + 45 feet (845 feet), under the slope of the mesa with 1000 to 1100 feet of overburden.

HFS 7, in which a single packer was used at 1200 lb/in^2, was vertical and was fractured in the zone from 65 to 71.5 feet, its maximum depth. Maximum pressure (P_c) reached was 440 lb/in^2 with rounded peak, a driving pressure (P_f) of 350 lb/in^2, and an instantaneous shut-in pressure (P_{si}) of 340 lb/in^2. The signatures of P_c and P_{si} were not clear; probably the rounded trace of P_c represented a preexisting natural fracture.

HFS 8 was a horizontal hole at CS 8 + 49 feet; it was fractured in two zones: from 37 to 43 feet with a straddle packer and from 65 to 105 feet, its maximum length, with a single packer. An attempt was made to fracture the 37-to-43-foot

Table 1

Hydrofracture Data

Hole No. (Orientation) Zone (ft)	Overburden (ft)	Breakdown P_c (lb/in²)	Frac/Driving P_f (lb/in²)	Inst. Shut-In P_{si} (lb/in²)
HFS 7 (V)	1100			
65 - 71.5		440 rounded	350	340
HFS 8 (H) N34°W	1050			
37 - 43		860	700	475
65 - 105 (TD)		750	650-700	450
Single packer				
HFS 9 (H) N60°E	1050			
38 - 44		750	450	300
52 - 58		800	500	Not recorded
71 - 101 (TD)		1250	550	425
Single packer				
HFS 10 (H) N26°E	1380			
37 - 43		1125	975	900
61 - 67		1150	875	875
87 - 93		1100	900	875
HFS 11 (H) S62°E	1380			
28 - 34		1250	875	850
47 - 53		1600	1000	900
85.5 - 91.5		1400	1200-1300	1000
HFS 12 (V)				
20 - 26	1400	675	700	675
35 - 41	1420	700	700	700
54 - 60	1435	875	800	675
74 - 80	1455	1375	1150	1050
HF 20 (H) N71°E	1435			
4.5 - 11.5		800	280	200
22.5 - 29.5		1100	730	650
42.5 - 49.5		1160	1000	800
62.5 - 69.5		1520	950	750
HF 39 (H) S19°E	1450			
17.5 - 22.5		1794	835	680
42.5 - 47.5		1670	812	698
72.5 - 77.5		1607	1025	750
HF 40 (H) N19°W	1435			
40 - 45		1674	767	719
50 - 55		1756	761	710
HF 45 (H) N52°W	1400			
31 - 41.5 (TD)		337*	116*	
Single packer			1220	1050
HF 46 (H) N15°E	1400			
18 - 22		1610	1300-1500	1200
30 - 37.5 (TD)		1702*	1175*	1078
Single packer				

*Related to explosive cavity

Table 2

12g Tuff Physical Properties Laboratory Tests

Sample Location	HFS 7,8,9	HFS 10,11,12
Bulk Density (g/cm^3)		
As received	1.99(1.94-2.12)	1.94(1.84-2.01)
Dry	1.67(1.59-1.82)	1.59(2.38-2.57)
Grain	2.50(2.44-2.57)	2.50(2.38-2.57)
Porosity (%)	32.7(28.7-35.9)	35.5(30.4-39.1)
Moisture Content (%)		
Natural state basis	16.1(11.4-19.3)	17.8(15.3-21.4)
Dry state basis	19.2(12.9-23.9)	21.7(18.4-27.3)
Unconfined Compressive Strength (lb/in^2)	3623(2000-4500)	2840(1470-6300)
Tensile Strength (lb/in^2)	190(29-324)	122(37-178)
Poisson's Ratio	0.25(0.196-0.292)	0.24(0.145-0.317)
Permeability (mD)	0.01; for HFS 9 only, as received	0.18; Oven Dry
Sonic Velocity (ft/s)		
Compressional	8325(7900-9100)	8300(7960-10000)
Shear	4465(4180-5060)	4628(4214-5281)

NOTE: 1. No data from HF 20,39,40,45,46.
2. Numbers in parentheses represent range.

zone with a packer set at 500 and 800 lb/in^2, but water leaked by the packer. When 1250 lb/in^2 was used in the packer, P_c was 860 lb/in^2, P_f was 700 lb/in^2, and P_{si} was approximately 475 lb/in^2. The single packer was set at 65 feet using 1450 lb/in^2. The P_c was 750 lb/in^2, P_f was approximately 650 to 700 lb/in^2, and P_{si} was approximately 450 lb/in^2.

HFS 9, a horizontal hole, was fractured in three zones: from 38 to 44 feet, 52 to 58 feet, and 71 to 101 feet total depth (TD). Packers were set with 1350 to 1450 lb/in^2. The 38- to 44-foot zone showed a P_c of 750 lb/in^2, a P_f of 450 lb/in^2, and a P_{si} of 300 lb/in^2. The 52- to 58-foot zone showed a P_c of 800 lb/in^2 and a P_f of 500 lb/in^2; P_{si} was not recorded. In the 71- to 101-foot zone, a single packer was set at 1450 lb/in^2; P_c was 1250 lb/in^2; P_f, 550 lb/in^2; and P_{si}, 425 lb/in^2.

HFS 9 was conventionally mined out along its length, and the trend of the fractures is N10°E to N15°E; the dip, 59°E to 64°E, with an average of N12°E, 60°E. The fractures crossed the hole axis at 50°, as a straight plane which formed an elliptical pattern at the hole surface, with no apparent turning of the fracture attitude away from the hole. The attitude of the fractures in all zones was consistent although, at the deepest zone, a single mechanical packer was used, and the several fractures seem to initiate at the packer. Fractures in all zones were approximately symmetrical around the hole; they extended up, down, and to both sides of the hole, commonly beyond the limits of mining. This is described further in Reference 1.

Data from HFS 10, 11, and 12 (1974)

The holes 10, 11, and 12 were an approximately orthogonal array of holes 100 feet deep, located near CS 27 + 35 feet, under the caprock of the mesa, with 1380 to 1450 feet of overburden.

HF 10 was a horizontal hole fractured in three zones: 37 to 43 feet, 61 to 67 feet, and 87 to 93 feet by using a straddle packer set with a pressure of 1500 to 1900 lb/in^2. The 37- to 43-foot zone had a P_c of 1125 lb/in^2, a P_f of 975 lb/in^2, and a P_{si} of 900 lb/in^2. The P_c record showed a rounded curve rather than a sharp break. The 61- to 67-foot zone showed a P_c of 1150 lb/in^2, a P_f of 875 lb/in^2, and a P_{si} of 875 lb/in^2 that had a very low decay rate. The packer setting was 1900 lb/in^2. The 87- to 93-foot zone showed a P_c of 1100 lb/in^2, a P_f of 900 lb/in^2, and a P_{si} of 875 lb/in^2 that had a very low decay rate. The packer setting was 1800 lb/in^2. Three pumpings were done; the last one leaked back into the tunnel.

HFS 10 was also conventionally mined out, and the fractures from the three zones trend consistently N44°E to N47°E, dip from 75°SE to 88°SE, with an average of N45°E, 85°SE. The fractures appeared to cross the hole in an elliptical path with no evidence that they changed direction away from the hole. The fractures in all zones extend up, down, and to both sides of the hole. The horizontal extent of the fractures was from 25 to 50 feet, but the observed vertical extent was limited to the approximately 11-foot tunnel height. Indications are, however, that fractures may not extend very far above or below the tunnel openings and are elongated in a horizontal direction.

Hydraulic fractures commonly intersected natural fractures and, in general, were not affected. However, at one location near the end of the green-dyed hydraulic fracture, where a natural fracture which was approximately perpendicular to the hydraulic fracture was encountered, the green dye followed along the natural fracture for approximately 4 inches then continued its original direction for several more feet. In two of the dyed hydraulic fractures, a nondyed extension of the fracture continued for several feet beyond the end of the visible dye.

HFS 11 was a horizontal hole fractured in three zones with a straddle packer set at 1800 lb/in^2. The 28- to 34-foot zone showed a P_c of 1250 lb/in^2, a P_f of 875 lb/in^2, and a P_{si} of 850 lb/in^2. The 47- to 53-foot zone showed a P_c of 1600 lb/in^2 with a sharp break, a P_f of 1000 lb/in^2, and a P_{si} of 900 lb/in^2 with a smooth but moderate pressure decay. Of three pumpings, the first had a leaky swivel, and the second showed a small leak into the tunnel. The first pump in the 85.5- to 91.5-foot zone showed the P_c as a level trace at 1300 lb/in^2 with a blip to 1400 lb/in^2, a P_f of from 1200 to 1300 lb/in^2, and a P_{si} of approximately 1000 lb/in^2. Five pumpings were done because the pump was operating erratically. However, most of the data are consistent.

HFS 12 was a vertical hole fractured in 4 zones with a packer pressure of 1800 lb/in^2. The record of the 20- to 26-foot zone showed the P_c as a rounded plateau of 675 lb/in^2 which increased on further pumping to a P_f of 700 lb/in^2 and

a P_{si} of 675 lb/in^2. The 35- to 41-foot zone was similar; the P_c had a rounded plateau of 700 lb/in^2, a P_f of 700 lb/in^2, and a P_{si} of 700 lb/in^2. The 54- to 60-foot zone had a P_c of 875 lb/in^2, a P_f of 800 lb/in^2, and a P_{si} of 675 lb/in^2. In the lowest zone, from 74 to 80 feet, with 1455 feet of overburden, the P_c was 1375 lb/in^2, the P_f was 1150 lb/in^2, and the P_{si} was selected as 1050 lb/in^2, which was considerably higher than the upper zones although reasonably consistent with the other two holes in this array, HFS 10 and 11.

Data from HF 20 (1977), HF 39, 40 (1978)

HF 20, 39, and 40 were collared near each other although all are approximately horizontal and do not form an orthogonal array. In HF 20, the new Sandia hydrofrac pumping system was first used. HF 20 was fractured in four zones. The zone from 4.5 to 11.5 feet had a packer setting of 1820 lb/in^2, a P_c of 800 lb/in^2, a P_f of 280 lb/in^2, and a P_{si} of 200 lb/in^2. Only one pumping was done because fluid was leaking from a fracture near the collar. The zone from 22.5 to 29.5 feet had a packer setting of 1680 lb/in^2, a P_c of 1100 lb/in^2, a P_f of 730 lb/in^2, and a P_{si} of 650 lb/in^2. Two pumping cycles were made, but the pump did not always operate properly. The zone from 42.5 to 49.5 feet had a packer setting of 1470 lb/in^2, a P_c of 1160 lb/in^2, a P_f of 1000 lb/in^2, and a P_{si} of 800 lb/in^2. The last zone, from 62 to 69 feet, had a packer setting of 1690 lb/in^2, a P_c of 1520 lb/in^2, a P_f of 950 lb/in^2, and a P_{si} of 750 lb/in^2.

HF 20 was mined out along the hole, and the trend of the fractures was N35°E to N42°E, with a dip from 87°SE to 90°. The dyed fractures extend 10 and 25 feet inside the tunnel, crossing the hole at approximately 30° with no detectable change of direction away from the hole. The fractures extend a short distance below the hole, less than 1 foot, but continue upward 5 to 6 feet into the back of the tunnel. Commonly, the fracture shows several strands, usually with a zone width of less than 0.1 foot.

HF 39 was a hole in the HF 20 drift. It was fractured in a number of zones, but only three will be reported on because of their proximity to HF 20 and HF 40. Packer pressures ranged from 920 lb/in^2 to 1000 lb/in^2. The 17.5- to 22.5-foot zone showed a P_c of 1794 lb/in^2, a P_f of 835 lb/in^2, and a P_{si} of 680 lb/in^2. The 42.5- to 47.5-foot zone showed a P_c of 1670 lb/in^2, a P_f of 812 lb/in^2, and a P_{si} of 698 lb/in^2. The 72.5- to 77.5-foot zone showed a P_c of 1607 lb/in^2, a P_f of 1025 lb/in^2, and a P_{si} of 750 lb/in^2.

HF 40 was also a horizontal hole in the HF 20 drift and was fractured in two zones as part of a hydrofrac-seismic experiment. Packer pressure was set at 1000 lb/in^2. The 40- to 45-foot zone had a P_c of 1674 lb/in^2, a P_f of 767 lb/in^2, and a P_{si} of 719 lb/in^2. The 50- to 55-foot zone showed a P_c of 1756 lb/in^2, a P_f 761 lb/in^2, and a P_{si} of 710 lb/in^2.

Data from HF 45 and 46 (1978)

HF 45 and HF 46 were horizontal drill holes, both in the same vicinity and drilled for residual stress explosive experiments.

HF 45 was fractured in one zone, from 31 to 41.5 feet, with a single packer at 31 feet pressurized to about 1000 lb/in^2. The fracture broke out of the drill hole and into the existing explosively formed cavity with a P_c of 337 lb/in^2, an initial P_f of 116 lb/in^2, which increased to 1220 lb/in^2 after the cavity was filled, and a P_{si} of 1050 lb/in^2. Thus these values are related to the residual stress from the explosion and are not representative of the in-situ stress state.

HF 46 was fractured in two zones. In the zone from 18 to 22 feet, believed to be far enough from the explosive cavity to be the "normal" in-situ stress field, a straddle packer pressurized to 1100 lb/in^2 was used; the P_c was 1610 lb/in^2, the P_f ranged from 1300 to 1500 lb/in^2, and the P_{si} was 1200 lb/in^2. In the region of the explosive cavity, from 30 to 37.5 feet (TD), a single packer set at 1100 lb/in^2 was used. This zone showed a P_c of 1702 lb/in^2, a P_f of 1175 lb/in^2, and a P_{si} of 1078 lb/in^2.

In the mineback of HF 46, the 18- to 22-foot zone was far enough from the explosive event so that the fracture would be governed by the in-situ stress field. Since the azimuth of the fracture was expected to be about 30° from the hole azimuth, it was desired to see how the azimuth of the fracture changed as a function of distance from the hole. A modified mineback procedure was used in which a shelf was initially cut 23 inches above the hole, the intercepted fracture mapped, and then the shelf progressively lowered first to 10, 7, and 4 inches above the hole, then to 6.5 and 10.5 inches below it. Figure 4 shows a cross-sectional view of the technique. Figure 5 shows a composite of these shelf maps at various distances above and below the center line of the drill hole. The figure shows the axis of the drill hole, the edge of the face below the shelf, the observed fractures, and selected strikes (azimuths). Well away from the hole, the fracture azimuth is N60°E, which is most likely controlled by the in-situ stress. Closer to the hole, it is N35°E at 23 inches away and, finally, N20°E at 4 inches from the center line of the hole. Note also the numerous stranding of the fracture.

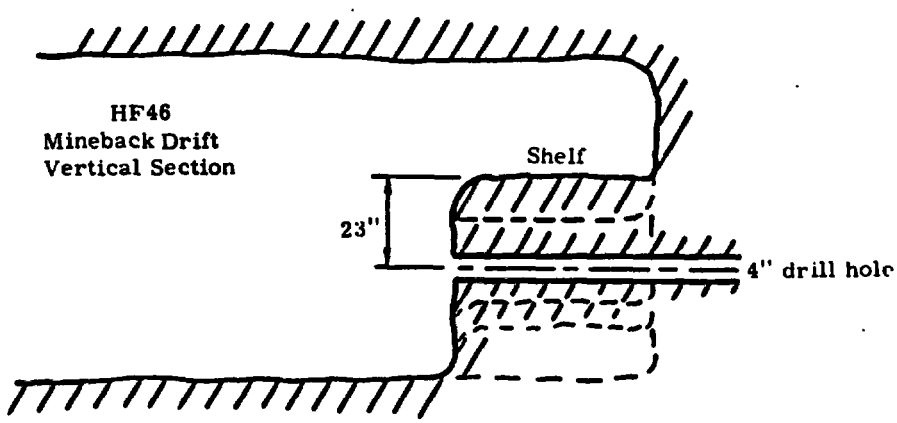

Figure 4. Mineback Procedure for HF 46 Fracture

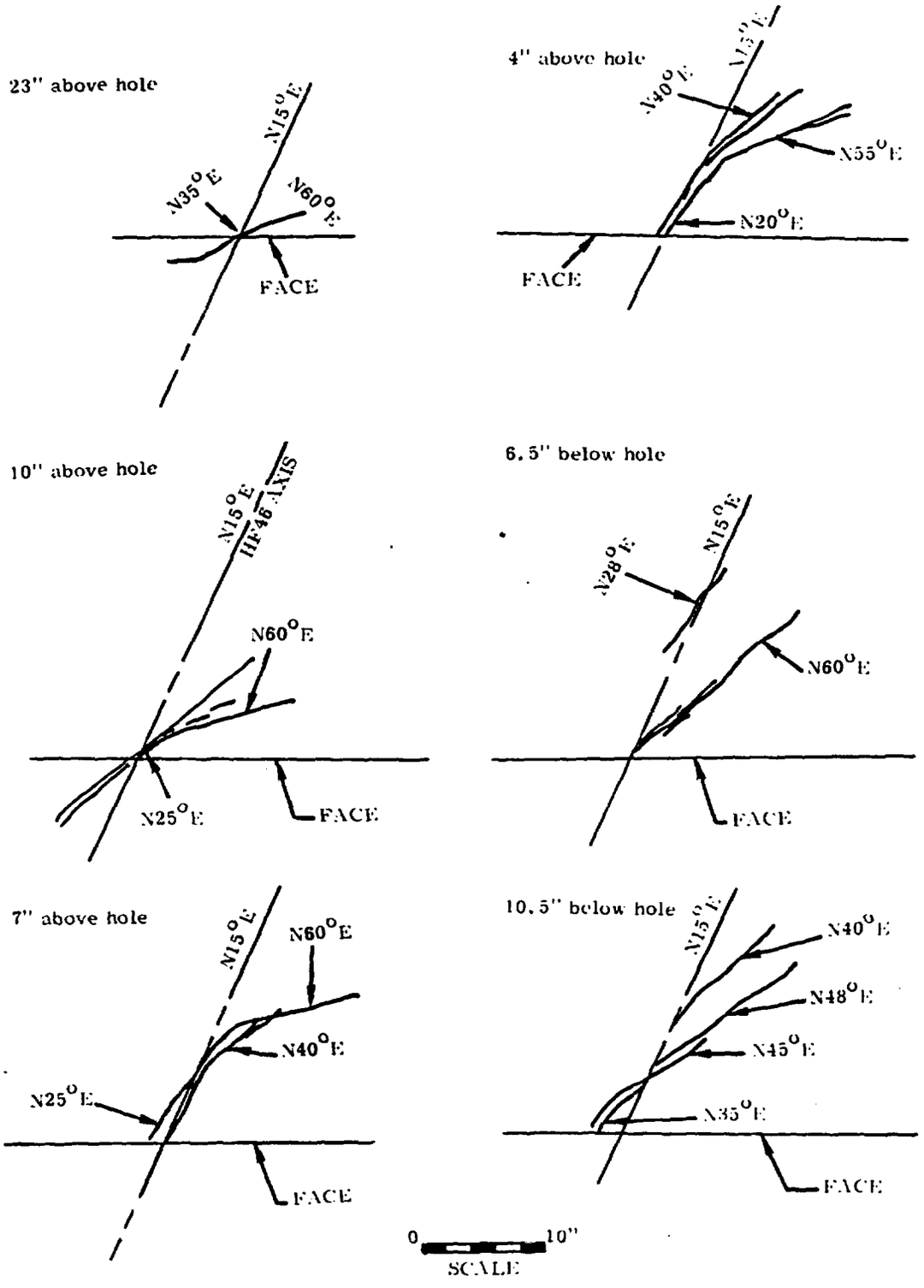

Figure 5. Top Views of Turning Fracture Observed on HF 46 Mineback

Stress Analysis

In Appendix B, expressions are derived for the stress and displacement fields in an infinite, linearly-elastic body containing an infinitely-long circular cylindrical cavity of radius R_o. The surface of the cavity is subjected to a uniform pressure, P, while a general uniform stress state prevails at infinity. In Appendix C, the uniform stress state at infinity is represented in terms of the three principal stresses at infinity through use of Euler's angles and the usual tensor transformations. Thus, the stress field at the surface of the cavity is determined in terms of the principal stresses at infinity and the angles which these stresses make in relation to the axis of the cavity.

Interest here is not on the direct problem of determining borehole stresses due to internal pressure and known in-situ stresses, but rather on the inverse problem. That is, given some information about the state of stress at the borehole, what are the in-situ stresses? Information available from hydrofrac tests is not sufficient to provide a unique solution to this inverse problem, even in the case of fracturing three mutually-orthogonal boreholes. As pointed out earlier, pressure data from a fracturing test provide only two pieces of information: a <u>critical</u> or <u>breakdown</u> pressure, P_c, at which the fluid pressure fractures the borehole, and the <u>shut-in</u> pressure, P_{si}, at which the fracture closes after fluid is no longer pumped into the open fracture. Depending on how the fracture surface is orientated with respect to the borehole, this shut-in pressure is equal to or slightly greater than the minimum principal in-situ stress, which is the stress normal to the fracture surface. It is generally assumed to be equal to the minimum principal in-situ stress. The breakdown pressure, P_c, depends on the principal stresses and their directions as well as on the tensile strength of the formation. And this accounts for the basic difficulty in trying to solve the inverse problem. Any number of combinations of principal stress magnitudes and directions can lead to the same P_c, and the critical point on the borehole surface where fracture initiates cannot be determined. A postfracture investigation of the borehole surface will reveal the final fracture line but will not indicate at what point and in what direction fracture initiated. The presence of the borehole itself alters the uniform stress field enough so that this fracture line is virtually useless in predicting fracture direction in the general case. Thus, even hydrofracing three mutually-orthogonal boreholes produces only four pieces of information at that point: three breakdown pressures and one shut-in pressure (generally taken as the average of the three shut-in pressures). While the magnitude of the minimum principal stress is obtained, its direction is not and little can be determined about the two remaining principal stresses and their directions. Because of these difficulties, the idea of hydrofracing a spherical cavity, which has no a priori orientation bias, rather than a cylindrical cavity has been advanced.[19] Analysis shows that the spherical cavity will fracture along a plane oriented normal to the minimum principal stress direction, and a postfracture investigation will determine the direction of this stress. The shut-in pressure will determine the magnitude of this minimum principal stress, and the breakdown pressure provides a relation between the magnitudes of the two other principal stresses which lie in the fracture plane. Other advantages in estimating in-situ stresses which are associated with the fracture of spherical cavities are detailed in Reference 19.

Another difficulty that arises when attempting to estimate in-situ stresses from hydrofrac pressure data is the effect on the stress field of the packers used to seal off the borehole interval. An analysis of these packer-induced stresses has recently been completed,[20] and these stresses are found to be tensile and proportional to the difference between the packer pressure and the hydraulic fracturing pressure. For typical packers, these stresses can become great enough to fracture the borehole under the effect of packer pressure alone before any hydraulic fracturing pressure is applied. When this occurs, a breakdown pressure may not be observed. If the initial packer pressure is not great enough to fracture the borehole, the packer-induced stresses will result in a measured breakdown pressure which is less than that predicted by analysis which ignores these stresses. In the fracture operations performed in G Tunnel, and reported on here, only the initial packer pressure was recorded, and, since this can differ significantly from the packer pressure at fracture, the analysis presented here ignores these packer-induced stresses.

In view of the analytical problems involved in utilizing pressure data from hydraulically-fractured cylindrical boreholes in the general case which we have delineated above, some assumptions or additional information are needed to estimate in-situ stresses. A usual assumption is that one of the principal stresses is vertical and equal to the overburden, that is, the weight of the geologic formation above the point where the in-situ stresses are to be determined. This assumption implies that the fracture plane will be either horizontal or vertical, depending on whether or not the overburden is the minimum principal stress. Since the hydraulically-fractured boreholes under discussion here are either vertical or horizontal, the assumption of a vertical principal stress implies that this stress is either parallel or normal to the borehole. Both situations allow a simplification of the stress expressions around the borehole. For a vertical borehole, this principal stress is parallel to the borehole, and the elementary expressions of Eq. (1) hold. The relevant equation for a horizontal borehole is developed in the subsection immediately following.

Additional information may also be obtained from postfracture observations. One example of this is to mineback along the borehole to the area of the fracture and determine the orientation of the fracture plane and thus the direction of the minimum principal stress. Several hydraulically-fractured boreholes in G Tunnel have been examined with mineback (Appendix A). The use of this information in estimating in-situ stresses is recorded in the results section of this report. In general, fracture planes at points in G Tunnel which lie under the level portions of the mesa are essentially vertical, indicating that the minimum principal stress is horizontal and that the assumption of a vertical principal stress in this region may be quite realistic. At points which lie under the sloping portion of the mesa, however, the fracture planes are inclined from the vertical, this inclination being away from the topography gradient and consistent in general trend with the theoretical analysis of overburden stress under inclined terrain (Appendix D). While consistent in general trend, the actual angular displacement of the fracture plane from the vertical is observed to be considerably greater than the analysis of Appendix D predicts. This is realistic since other in-situ effects besides overburden are certainly operating in this situation.

Stresses at a Horizontal Borehole with One Principal Stress Vertical

The level of generality of the borehole stresses presented in Appendices B and C makes them difficult to work with, so here attention is restricted to the usual situation in G Tunnel where the borehole is horizontal and one principal stress is vertical, i.e., normal to the axis of the borehole. In the notation of Appendix C, with the borehole directed along the z' axis, this vertical principal stress is denoted as σ_{xx} in the direction x. Then, in the transformation A of Eq. (C2), take

$$\phi = 0, \ \psi = 0 \tag{2}$$

and, denoting the principal stresses of Eq. (C6) by

$$\sigma_{xx} = \sigma_1 \ , \ \sigma_{yy} = \sigma_2 \ , \ \sigma_{zz} = \sigma_3 \ , \tag{3}$$

obtain

$$\begin{aligned} \bar{\sigma}_{xx} &= \sigma_1 \ , \ \bar{\sigma}_{xy} = 0 \ , \ \bar{\sigma}_{xz} = 0 \ , \\ \bar{\sigma}_{yy} &= \sigma_2 \cos^2\alpha + \sigma_3 \sin^2\alpha \ , \\ \bar{\sigma}_{yz} &= -(\sigma_2 - \sigma_3)\sin\alpha \cos\alpha \ , \\ \bar{\sigma}_{zz} &= \sigma_2 \sin^2\alpha + \sigma_3 \cos^2\alpha \ . \end{aligned} \tag{4}$$

The geometry under discussion is shown in Figure 6. Measuring the angle Θ around the borehole from the vertical x = x' axis, Eq. (B25) with Eq. (4) gives the non-zero borehole surface stresses

$$\begin{aligned} \sigma_{\Theta\Theta} &= -P + \sigma_1 + \sigma_2 \cos^2\alpha + \sigma_3 \sin^2\alpha - 2(\sigma_1 - \sigma_2 \cos^2\alpha - \sigma_3 \sin^2\alpha)\cos 2\Theta \ , \\ \sigma_{zz} &= \sigma_2 \sin^2\alpha + \sigma_3 \cos^2\alpha - 2\nu(\sigma_1 - \sigma_2 \cos^2\alpha - \sigma_3 \sin^2\alpha)\cos 2\Theta \ , \\ \sigma_{\Theta z} &= -2(\sigma_2 - \sigma_3)\sin\alpha \cos\alpha \cos\Theta \ . \end{aligned} \tag{5}$$

If the minimum principal stress is the vertical stress σ_1, Eq. (5) shows that the minimum stress at the borehole surface is $\sigma_{\Theta\Theta}$ at $\Theta = \pi/2$, and the resulting fracture plane will be horizontal, or normal to σ_1. This situation is of little interest in G Tunnel, so it is now assumed that σ_1 is not the minimum principal stress and, without loss of generality, the minimum stress is denoted as σ_3, that is

$$\sigma_3 < \sigma_1 \ , \ \sigma_3 < \sigma_2 \ , \tag{6}$$

and the angle α is the angle of this stress direction with respect to the borehole axis. That is, α is the angle of the normal to the fracture plane from the axis of the borehole. From Eq. (B28), the pressure P required to provide a $\sigma_{min} = -T$, where T is the tensile strength of the formation, at any point Θ around the borehole is given by

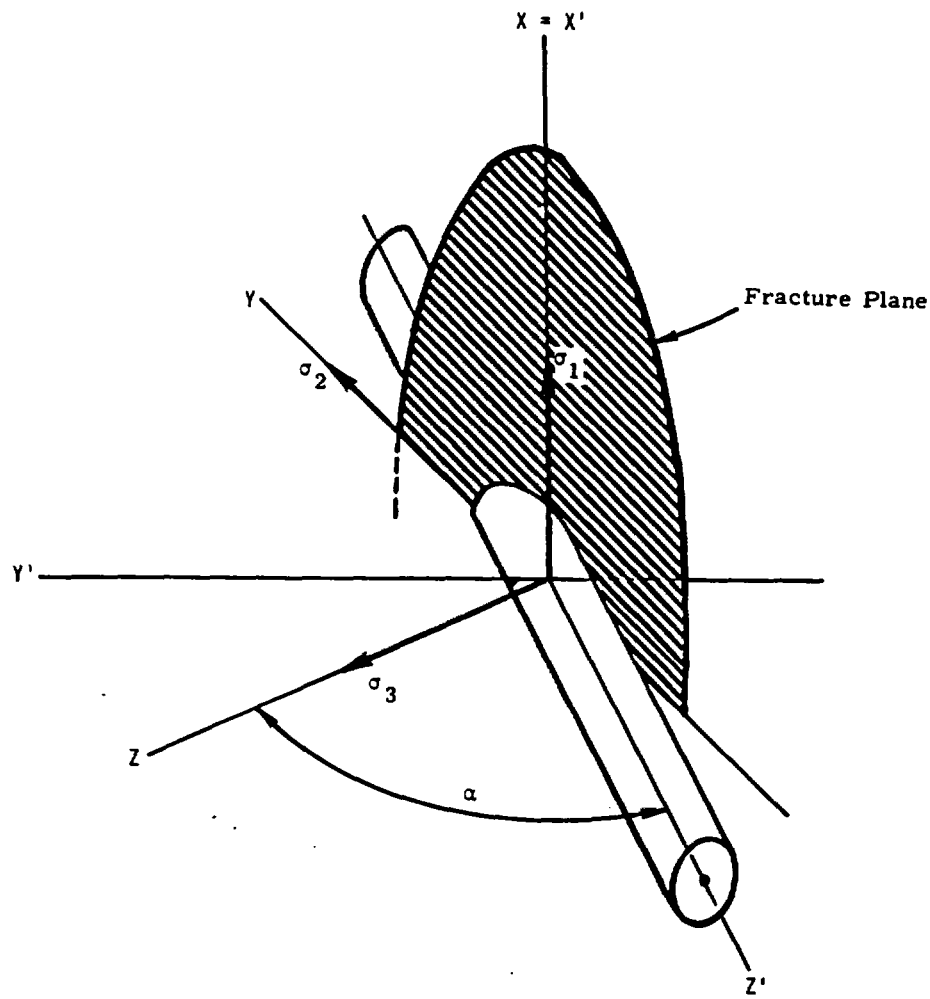

Figure 6. Geometry of Borehole with One Principal Stress Normal

$$\hat{P} = \frac{\left\{ \begin{array}{l} [T - (1 + \nu)C \cos 2\Theta]^2 + 2(C + \sigma_3 - \sigma_1)(C + \sigma_2 - \sigma_1)(1 + \cos 2\Theta) \\ \quad - [\sigma_2 + \sigma_3 - \sigma_1 + C + (1 - \nu)C \cos 2\Theta]^2 \end{array} \right\}}{[T - \sigma_1 + \sigma_2 + \sigma_3 + C - 2\nu C \cos 2\Theta]} \tag{7}$$

where

$$\hat{P} = P - \sigma_1 - \sigma_2 - \sigma_3 ,$$

$$C = \sigma_1 - \sigma_2 \cos^2\alpha - \sigma_3 \sin^2\alpha . \tag{8}$$

This relationship gives the P required to establish $\sigma_{min} = -T$ at any angle θ around the borehole. Now, it is necessary to find the minimum P on the interval $0 \leq \theta \leq \pi/2$. Differentiating $\hat{P}$ gives

$$\frac{1}{4}\frac{\partial P}{\partial \theta} = \frac{\left\{\begin{array}{l} 4\nu^2C^3 \cos^2 2\theta - 4\nu C^2 \cos 2\theta(T - \sigma_1 + \sigma_2 + \sigma_3 + C) \\ + C(T - \sigma_1 + \sigma_2 + \sigma_3 + C)^2 \\ - (C + \sigma_3 - \sigma_1)(C + \sigma_2 - \sigma_1)\,[(1 + 2\nu)C + T - \sigma_1 + \sigma_2 + \sigma_3] \end{array}\right\} \sin 2\theta}{[T - \sigma_1 + \sigma_2 + \sigma_3 + C - 2\nu C \cos 2\theta]^2} \qquad (9)$$

This expression goes to zero at $\theta = 0, \pi/2$, which indicates that fracture of the borehole will initiate at one of these points. There is a theoretical possibility of fracture initiating at some other point defined by the zeros of the bracketed term in Eq. (9) but the numerical results which have been carried out indicate that under conditions for which this will occur, the minimum P is very close to the P required for fracture to initiate at $\theta = 0$ or $\theta = \pi/2$. Figure 7 shows values of the minimum stress, σ_{min}, at points around the borehole, $0 \leq \theta \leq \pi/2$, for several values of the borehole orientation angle α. Each of these curves is for the minimum pressure P required to provide a maximum tensile stress T of 300 lb/in^2 to produce fracture at some point around the borehole.*

The in-situ principal stresses for the example of Figure 7 are $\sigma_1 = 1100$ lb/in^2, $\sigma_2 = 1700$ lb/in^2, and $\sigma_3 = 900$ lb/in^2, which are approximately those found in G Tunnel near the triad of boreholes HFS 10, 11, and 12. Also shown in Figure 7 is the angle γ, given by Eq. (B27), which the minimum stress surface makes with the axis of the borehole (Figure B1). It can be observed that the location of the point on the borehole where $\sigma_{min} = -T$ shifts from $\theta = \pi/2$ to $\theta = 0$ occurs at an orientation angle α of $\alpha \cong 55°$. From the plot of γ versus θ it can be seen that when $\sigma_{min} = -T$ at $\theta = \pi/2$, $\gamma = 0$, which indicates that fractures initiating at this point would be expected to run parallel to the borehole axis. On the other hand, when $\sigma_{min} = -T$ at $\theta = 0$, $\gamma \neq 0$, and these fractures are expected to have some angle less than $(90° - \alpha)$ from the borehole axis. In either case, the fracture at the borehole initiates at an angle different from the angle at which the final fracture surface grows away from the borehole which is normal to σ_3 and given by $(90° - \alpha)$. Thus, the fracture twists as it grows out into the formation from the borehole. This effect is substantiated by the mineback observations of HF 46, shown in Figure 5, and is discussed in more detail in the results section of this report.

---

*A value of 300 lb/in^2 is used in this report as the effective tensile strength of the tuff when subjected to internal pressurization. The values shown in Table 2 are from uniaxial tensile tests and are about one-half the above value. Preliminary work to measure T gave values ranging from 100 to 700 lb/in^2. The low values were associated with natural fractures; the high values came from pressurizations on the tunnel ribs where the tuff had not been fully relieved from the in-situ stress. Tuff samples that had been relieved on three sides and were free from natural fractures gave values in the 250 to 350 lb/in^2 range. Terra Tek[16] has measured a T value by pressurizing cylindrical samples from N Tunnel, Area 12, and found an average tensile strength value of 435 lb/in^2.

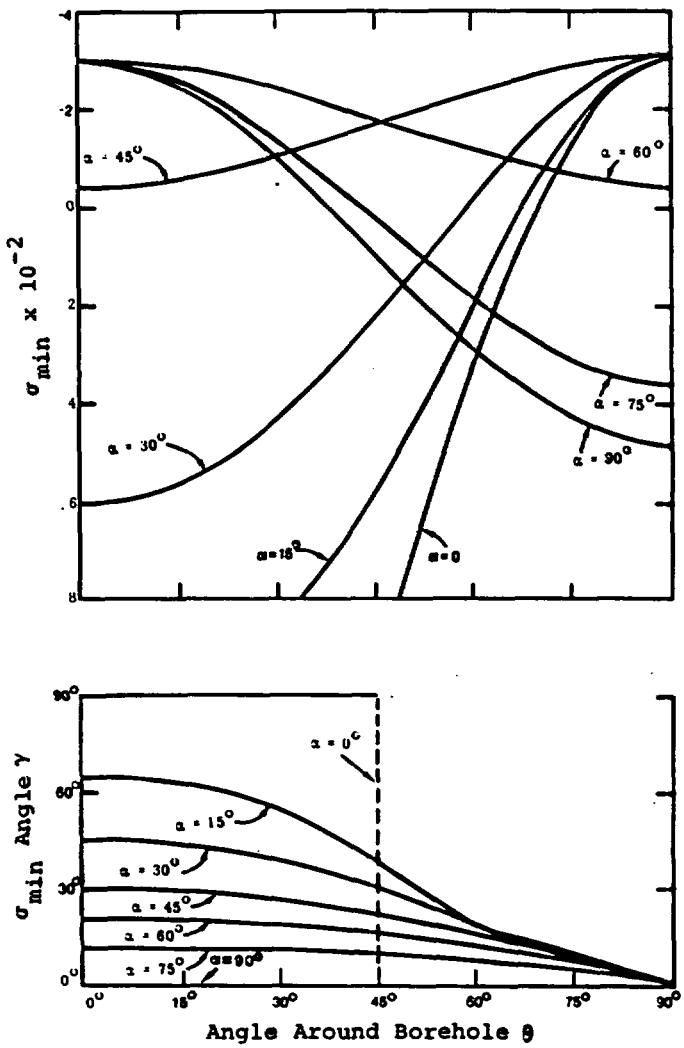

Figure 7. Plot of σ_{min} versus Position θ around Borehole for Several Angles α

The minimum pressure P required to provide a $\sigma_{min} = -T$ at some point on the borehole surface is the critical or breakdown pressure P_c, and for the example of Figure 7, this pressure is shown as a function of borehole orientation angle α in Figure 8. Note that the same critical pressure, P_c, occurs for two different orientation angles, α, and thus demonstrates one of the difficulties, discussed earlier, which are associated with the inverse problem of determining in-situ stresses from hydrofrac pressure data. While it is true that fracture initiates at different points around the borehole for each of these two angles, a postfracture investigation of the borehole will reveal only a completely fractured surface, the point of initiation being lost. Clearly, other combinations of σ_1, σ_2, σ_3, and α could result in the same P_c of Eq. (7).

If the fracture initiates at $\theta = \pi/2$, then the minimum pressure P_c is given by

$$P_c = T + 2\sigma_1 + C \ , \tag{10}$$

and the angle γ of the fracture from the borehole axis shown in Figure B1 (Appendix B), is $\gamma = 0$. If the fracture initiates at $\theta = 0$, the minimum pressure P_c is given by

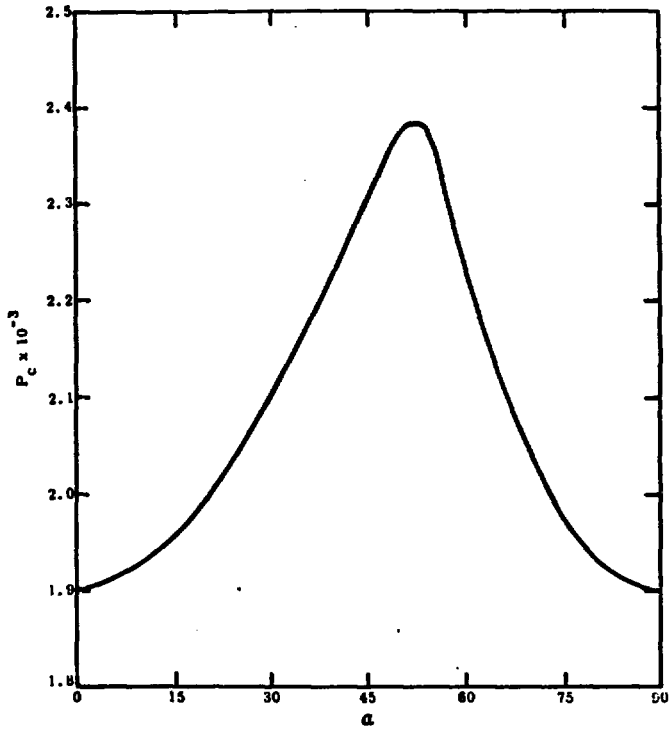

Figure 8. Critical Pressure P_c versus Borehole Orientation Angle α

$$P_c = T + 2\sigma_1 - 3C - \frac{4\cos^2\alpha \ \sin^2\alpha(\sigma_2 - \sigma_3)^2}{[E + (1 - 2\nu)C]} , \tag{11}$$

and the angle γ of the fracture is

$$\tan \gamma = \frac{(\sigma_2 - \sigma_3)\sin 2\alpha}{[E + (1 - 2\nu)C]} , \tag{12}$$

where

$$E = T - \sigma_1 + \sigma_2 + \sigma_3 . \tag{13}$$

Equation (12) shows the complex relation that exists between the fracture angle γ and the principal stress direction α and provides another example of the difficulty of estimating the in-situ stress field from the pressure data alone.

Results

In this section, the analysis of the previous section and Appendices B and C is applied to the selected hydrofrac pressure data to obtain estimates of the in-situ stresses at these selected locations. A summary of the in-situ stresses in G Tunnel, as determined from analysis of all hydrofrac tests performed, is included in the Summary section.

Analysis of HFS 7, 8, and 9

This triad of boreholes is located under the slope of the mesa, east of the top edge. As shown in Appendix D, the theoretical fracture plane for this area is not vertical but inclined up and to the west. The three boreholes are approximately orthogonal to each other, HFS 7 being vertical and HFS 8 and 9 horizontal. Mineback of HFS 9 shows that the fracture plane is inclined at 30° from the vertical in essentially a westerly direction, and the geographic orientation of a horizontal line on the fracture plane is N14°E. While the angle of inclination is considerably greater than that predicted (Appendix D), the inclination is in the proper direction, and the horizontal geographic orientation is approximately perpendicular to the mesa gradient as expected.

The direction of the fracture plane defines the direction of the minimum principle in-situ stress since this stress is perpendicular to the fracture plane. With the direction of this stress known, two of the three Euler angles are determined, and the orientation of this minimum stress with respect to the axis of the three boreholes is known. The importance of knowing the direction of the fracture plane in order to determine the in-situ stresses should be emphasized. The magnitude of the minimum principal stress is approximately equal to the shut-in pressure, and, for this triad of boreholes, an average is used from the three shut-in pressures, which gives $\sigma_{min} = 470$ lb/in^2. The remaining two principal stresses must lie in the plane of the fracture.

For this inclined fracture plane, none of the boreholes are aligned normal to any of the three principal stresses, so the entire analysis of Appendix C must be used. A consistent set of principal stresses is obtained if it is assumed that one of the stresses in the fracture plane is horizontal, the other is then perpendicular to it. With this assumption, the following calculations are made for each of the three boreholes.

1. For the vertical borehole HFS 7, $\alpha = 60°$, $\phi = \psi = 0$, and $\sigma'_{xx} = \sigma_2$ $\sigma'_{yy} = \sigma_1$, $\sigma'_{zz} = \sigma_3 = 470$ lb/in^2 in Eq. (C5) to get the uniform stress field referred to the cylindrical coordinates of the borehole. Equations (B25) and (B28), with $P = 550$ lb/in^2, $\nu = 1/4$, and $T = 300$ lb/in^2, provide a relation between σ_1 and σ_2.

2. For the horizontal borehole HFS 8, whose axis has direction N34°W, $\alpha = -60°$, $\phi = -48°$, $\psi = 0$, and $\sigma'_{xx} = \sigma_2$, $\sigma'_{yy} = \sigma_1$, $\sigma'_{zz} = \sigma_3 = 470$ lb/in^2 in Eq. (C5), then the coordinates and stresses are relabeled such that $x \to z$, $y \to x$, $z \to y$ to get the uniform stress field referred to the cylindrical coordinates of the borehole. Equations (B25) and (B28), with $P = 775$ lb/in^2, $\nu = 1/4$, and $T = 300$ lb/in^2, then provide a second relation between σ_1 and σ_2.

3. For the horizontal borehole HFS 9, whose axis is directed N60°E, $\alpha = -60°$, $\phi = 46°$, $\psi = 0$, and $\sigma'_{xx} = \sigma_2$, $\sigma'_{yy} = \sigma_1$, $\sigma'_{zz} = \sigma_3 = 470$ lb/in^2 in Eq. (C5), the coordinates and stresses are relabeled such that $x \to z$, $y \to x$, $z \to y$ to get the uniform stress field referred to the cylindrical coordinates of the borehole. Equations (B25) and (B28), with $P = 788$ lb/in^2, $\nu = 1/4$, and $T = 300$ lb/in^2, then provide a third relation between σ_1 and σ_2.

Because of the unreliable and incomplete results from the pressure data of HFS 7, the most reliable results will be obtained from the stress relations for HFS 8 and 9. Results of this analysis indicate that a consistent in-situ stress field can be obtained which is

$$\sigma_1 = 1283 \text{ lb/in}^2 , \ \sigma_2 = 800 \text{ lb/in}^2 , \ \sigma_3 = 470 \text{ lb/in}^2 , \qquad (14)$$

where σ_1 lies in the vertical plane intersected by the fracture plane, σ_2 lies in the horizontal plane intersected by the fracture plane, and σ_3 is normal to the fracture plane. The orientation of these stresses with respect to the fracture plane is shown in Figure 9.

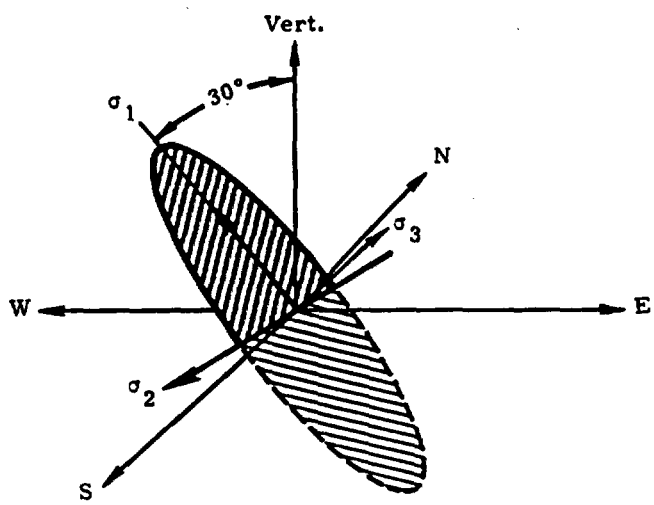

Figure 9. Orientation of Fracture Plane and Principal Stresses, HFS 7, 8, and 9

Using these stresses in the analysis for HFS 7 shows that a breakdown pressure $P = 550$ lb/in^2 is required to provide the maximum tensile stress of 300 lb/in^2 to fracture the borehole.

The slope of the mesa directly above this triad of boreholes is approximately 35° up and to the west (see Figure 13). Using this angle, an average density of $\rho = 1.99\ g/cm^3$ and an average depth of 1060 feet, the vertical uniaxial strain analyses of Appendix D, Case 2, Eq. (D11), provide

$$\sigma_1 = \sigma_{max} = 1173\ lb/in^2 ,$$

$$\sigma_3 = \sigma_{min} = 284\ lb/in^2 ,$$

$$\sigma_2 = \nu(\sigma_1 + \sigma_3) = 364\ lb/in^2 . \tag{15}$$

The angle of inclination of σ_1 from the vertical $|\gamma|$ is obtained from Eq. (D12) and found to be

$$|\gamma| = 17.5° . \tag{16}$$

The vertical component of the normal stress, σ_v, associated with the principal stress system of Eq. (14) is $\sigma_v = 1080\ lb/in^2$, while the vertical component σ_{VOB} associated with the overburden stress system of Eq. (15) is $\sigma_{VOB} = 1093\ lb/in^2$. Thus, while the simple overburden theory of Appendix D provides a relatively close approximation to the vertical component of the normal stress, σ_v, and the shifted overburden stress, σ_1, the other two principal stresses and the angle of inclination, γ, of the shifted overburden stress are considerably different.

Analysis of HFS 10, 11, and 12

These three boreholes are located well under the flat portion of the mesa and are approximately orthogonal to each other, HFS 10 and 11 being horizontal and HFS 12 vertical. The fracture plane is expected to be essentially vertical, and minebacking of HFS 10 verifies this. The geographic orientation of the vertical fracture plane is N46°E, and the minimum principal stress is horizontal with direction N44°W. From the average shut-in-pressure for these three boreholes, $\sigma_{min} = 860\ lb/in^2$ is obtained.

The remaining two principal stresses lie in the fracture plane, and a reasonable assumption is that one is vertical and the other horizontal. Thus, with this assumption, one principal stress is normal to the horizontal boreholes HFS 10 and 11, and both can be analyzed with the simplified equations of the previous section. Since the vertical stress is parallel to the vertical borehole and the maximum principal stress is normal to it, the elementary relation of Eq. (1) is applicable to the analysis of HFS 12 which provides

$$\sigma_2 = -P_c + 3\sigma_3 + T . \tag{17}$$

Using $P_c = 990\ lb/in^2$, $\sigma_3 = 810\ lb/in^2$, $T = 300\ lb/in^2$,

$$\sigma_2 = 1740\ lb/in^2 .$$

The axis of the horizontal borehole HFS 10 is directed N26°E. From the shut-in-pressure data, $\sigma_3 = 860$ lb/in^2 and taking

$$\alpha = -70° \ , \ P_c = 1125 \text{ lb/in}^2 \ , \ \nu = 1/4 \ , \ T = 300 \text{ lb/in}^2 \ ,$$

in Eq. 5, it is found that the maximum stress occurs at $\theta = 0$. A relationship between σ_1 and σ_2 then gives

$$\sigma_1 = 1/2 \left\{ (3012 + 2.235\sigma_2) - [2.456 \times 10^6 - 5.364\sigma_2 \times 10^3 + 5.653\sigma_2^2]^{1/2} \right\} , \qquad (18)$$

and, at $\sigma_2 = 1740$ lb/in^2, this provides

$$\sigma_1 = 1850 \text{ lb/in}^2 \ ,$$

which is an unrealistic number. The relation for σ_1 is relatively insensitive to values of σ_2 because of the small angle, 20°, between the borehole and the fracture plane. For example, σ_1 changes from 1825 lb/in^2 to 1850 lb/in^2 as σ_2 changes from 1200 lb/in^2 to 1800 lb/in^2. The pressure data of Table 1 for the three hydrofracs performed in this borehole is very consistent and must be considered reliable. It is felt that packer-induced stresses are responsible for this unrealistic value of σ_1 since the packers in this borehole were initially pressurized to 1800 to 1900 lb/in^2, which is very high. This unrealistic value of σ_1 has been ignored.

The axis of horizontal borehole HFS 11 is directed S62°E. From the pressure data, $\sigma_3 = 860$ lb/in^2 and taking

$$\alpha = 18° \ , \ P_c = 1425 \text{ lb/in}^2 \ , \ \nu = 1/4 \ , \ T = 300 \text{ lb/in}^2$$

in Eq. (5), it is found that the maximum stress occurs at $\theta = \pi/2$. The relation between σ_1 and σ_2 becomes

$$3\sigma_1 - .904\sigma_2 = 1207 \text{ lb/in}^2 \ , \qquad (19)$$

and, at $\sigma_2 = 1740$ lb/in^2 , this provides

$$\sigma_1 = 927 \text{ lb/in}^2 \ .$$

Thus, a consistent set of in-situ stresses for this triad of boreholes is found to be*

$$\sigma_1 = 930 \text{ lb/in}^2 \ , \ \sigma_2 = 1740 \text{ lb/in}^2 \ , \ \sigma_3 = 860 \text{ lb/in}^2 \ , \qquad (20)$$

---

*Using the analysis in Reference 20 for packer-induced stresses, the following set of stress values is arrived at.

$\sigma_1 = 1000$ lb/in^2 , $\sigma_2 = 1080$ lb/in^2, and $\sigma_3 = 860$ lb/in^2 ,
with directions the same as given above.

where σ_1 is directed vertically, σ_2 is directed horizontally in the plane of the fracture, N46°E, and σ_3 is directed horizontally and normal to the fracture plane N44°W. The orientation of these stresses with respect to the fracture plane is shown in Figure 10.

Using an average density of 1.94 g/cm^2 from Table 2 and an overburden depth of 1380 feet, the vertical overburden stress σ_{ob} at this point is found to be σ_{ob} = 1160 lb/in^2, which differs by 25% from the calculated vertical principal in-situ stress σ_1.

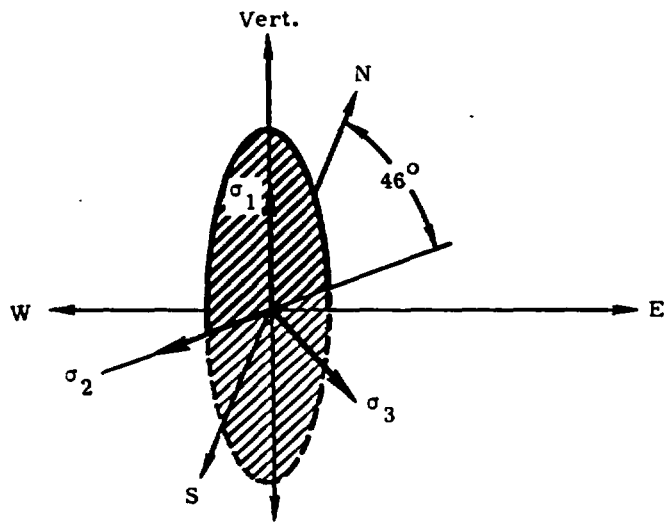

Figure 10. Orientation of Fracture Plane and Principal Stresses, HFS 10, 11, and 12

Analysis of HF 20, 39 and 40

These three boreholes are all horizontal, HF 39 and 40 being essentially parallel to each other and orthogonal to HF 20. HF 39 is more than 200 feet long, and nine successful hydrofracs were performed along its length. Here, only data from the three hydrofracs which were closest to HF 20 and 40 are considered since this data was consistent with the fracture data of HF 40. An analysis of all nine fractures of HF 39 has been reported in a memo.[23]

These three boreholes are located under the flat portion of the mesa at a depth of 1435 feet. Under these conditions, the fracture plane is expected to be vertical, and this has been verified by the mineback of HF 20. Results of the mineback show the fracture plane to be vertical and oriented N42°E. The average shut-in-pressure for these three boreholes gives the minimum in-situ stress of σ_{min} = 720 lb/in^2, which is normal to the fracture plane and thus horizontal with orientation N48°W. The axis of HF 20 is N71°E. Assuming σ_1 to be a vertical and σ_2 a horizontal stress normal to σ_3 and putting

$$\alpha = 61° \ , \ P_c = 1300 \text{ lb/in}^2 \ , \ \nu = 1/4 \ , \ T = 300 \text{ lb/in}^2$$

in Eq. (5), the maximum stress in HF 20 is found to occur at $\theta = 0$. At this point, the relation between σ_1 and σ_2 becomes

$$\sigma_1 = 1/2 \left\{(2143 + 2.469\sigma_2) - [3.68 \times 10^6 - 6.51\sigma_2 \times 10^3 + 6.87\sigma_2^2]^{1/2}\right\}. \quad (21)$$

A second relation between σ_1 and σ_2 is obtained from the results of HF 39 and 40.

The axis of HF 39 and 40 are both N19°W. Setting

$$\alpha = -29° \ , \ P_c = 1700 \ \text{lb/in}^2 \ , \ \nu = 1/4 \ , \ T = 300 \ \text{lb/in}^2$$

in Eq. (5), the maximum stress again occurs at $\theta = 0$. At this point, the relation between σ_1 and σ_2 becomes

$$\sigma_1 = 1/2 \left\{(977 + 3.53\sigma_2) - [10.61 \times 10^6 - 14.13\sigma_2 \times 10^3 + 6.88\sigma_2^2]^{1/2}\right\}. \quad (22)$$

Simultaneous solution of Eqs. (21) and (22) gives the vertical stress $\sigma_1 = 1292$ lb/in^2 and the horizontal stress $\sigma_2 = 975$ lb/in^2. The in-situ stresses in the neighborhood of HF 20, 39, and 40 are

$$\sigma_1 = 1292 \ \text{lb/in}^2 \ , \ \sigma_2 = 975 \ \text{lb/in}^2 \ , \ \sigma_3 = 720 \ \text{lb/in}^2 \ , \quad (23)$$

where σ_1 is directed vertically, σ_2 is directed horizontally in the plane of the fracture N42°E, and σ_3 is directed horizontally and normal to the fracture plane N48°W. The orientation of these stresses with respect to the fracture plane is shown in Figure 11.

This region is located approximately 200 feet from the triad of holes HFS 10, 11, and 12, and using the average density for these as listed in Table 2 and an overburden depth of 1435 feet gives a vertical overburden stress at this point of $\sigma_{OB} = 1206$ lb/in^2. This vertical overburden stress is within 7% of the calculated vertical principal in-situ stress σ_1.

Analysis of HF 45 and 46

These two boreholes are horizontal and were utilized in conjunction with the high-explosive (HE) shots RS 5 and 6. The end of the HF 45 borehole is about 15 inches below the RS 5 cavity, and the end of the HF 46 borehole is 2 to 3 feet below the RS 6 cavity. The residual compressive stress cage around the two cavities resulting from the HE shots alters the in-situ stress field considerably at the ends of HF 45 and 46 so the pressure data from the hydraulic fracture operations performed at the ends of these boreholes do not relate to the far-field uniform in-situ stresses in any meaningful way. The fracturing operation performed in the interval 17.6 to 22.4 feet in HF 46 is probably far enough away from both the RS 5 and RS 6 cavities that this region is not affected by the residual

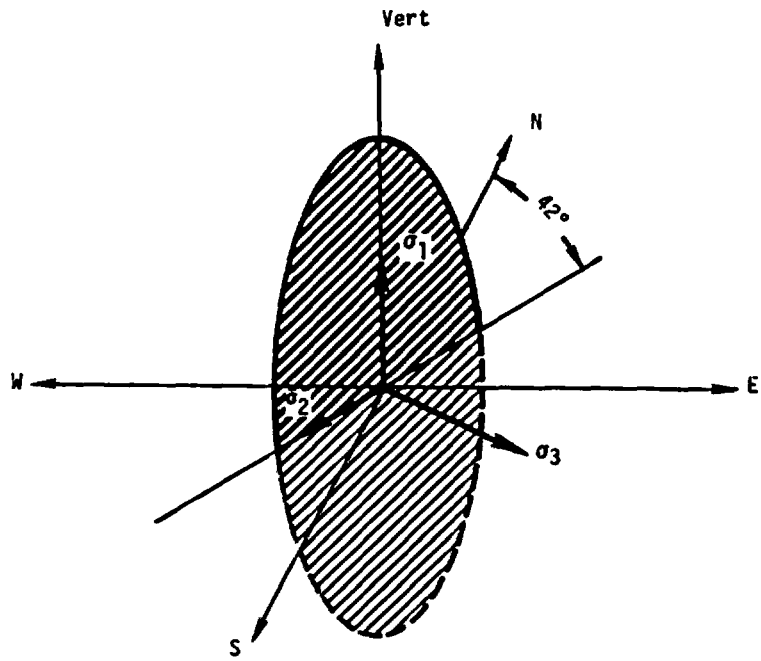

Figure 11. Orientation of Fracture Plane and Principal Stresses, HF 20, 39, and 40

compressive stress cage set up around the cavities. The pressure-time record for this test is shown in Figure 12 and demonstrates the type of anomalous behavior which can occur during hydraulic fracturing operations. While this pressure data provides unrealistic values for the in-situ stress field, observations made during mineback provide some interesting information about the fracture propagation from the borehole and about the effects of packer-induced stresses.

Theoretical analyses of borehole stresses indicate that the direction of the initial fracture at the borehole surface will not be the same as the direction of the fracture in the far field. Thus, the fracture plane is expected to change direction as the fracture grows away from the borehole. This reorientation is localized since the borehole induced stresses decay as $(Ro/r)^2$, as shown in Eqs. (B16) to (B21) of Appendix B. To verify this twisting of the fracture plane, HF 46 was mined back in such a way as to observe any changes in fracture direction. In the pressurized region 17.5 to 22.4 feet into the borehole, horizontal cuts about 2 feet deep were made, starting 23 inches above the borehole center line, and the fracture direction on each of the horizontal faces was observed. Figure 5 shows how the fracture plane projected on these faces twists as it grows vertically from the borehole, the cracks initiating at an angle of 5° to 25° from the axis of the borehole, finally reaching an angle of 45° (N60°E) at distances several borehole radii from the center line. The following analysis indicates that for the assumed in-situ stress field in this neighborhood, fractures should initiate at the top and bottom of the borehole in a direction 33° from the axis, the fracture direction twisting as it grows vertically, finally reaching 45° in the far field.

A second important effect, mainly that of fracture initiation at the packer, was observed during mineback. The face shown in Figure 5 is at 16.1 feet into the

borehole which is under the packer and about 1.5 feet from the packer end at 17.6 feet. The pressure-time record for this fracture operation (Figure 12), along with observations at mineback, indicate that the initial fracture started at the packer and grew slightly, probably moving under the packer but unable to continue in that direction at the pressure of initial fracture. Subsequent increases in the hydraulic fracturing pressure then propagated the crack in the usual way. This effect is consistent with the effect of packer-induced stresses which have been investigated by Warren,[20] the results of which have been incorporated into the following stress analysis of HF 46.

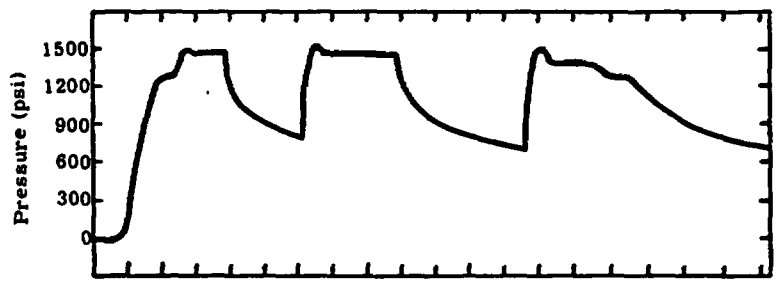

time - 10 seconds between marks

(a) Pressure #1 (at collar)

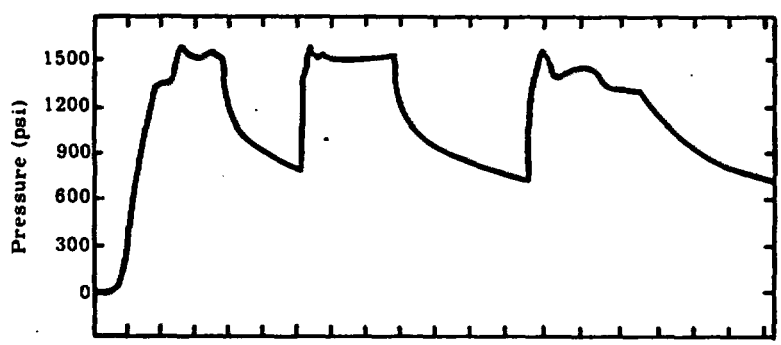

time - 10 seconds between marks

(b) Pressure #2 (at packer)

Figure 12. Pressure-Time Record for HF 46, Zone R8 -- 22 Feet

In the absence of other information, principal stresses are taken to be

$$\sigma_1 = 1200 \text{ lb/in}^2 \text{ vertical}$$

$$\sigma_2 = 1600 \text{ lb/in}^2 \text{ horizontal N60°E}$$

$$\sigma_3 = 900 \text{ lb/in}^2 \text{ horizontal N30°W} , \tag{24}$$

which are consistent with other results in this area of G Tunnel. The axis of HF 46 is horizontal with direction N15°E. Taking $\alpha = -45°$ in Eq. (4) gives the uniform stress field with respect to the borehole axis z as

$$\sigma^o_{xx} = \bar{\sigma}_{xx} = 1200 \text{ lb/in}^2 ,$$

$$\sigma^o_{xy} = \bar{\sigma}_{xy} = 0 ,$$

$$\sigma^o_{xz} = \bar{\sigma}_{xz} = 0 ,$$

$$\sigma^o_{yy} = \bar{\sigma}_{yy} = 1250 \text{ lb/in}^2 ,$$

$$\sigma^o_{yz} = \bar{\sigma}_{yz} = 350 \text{ lb/in}^2 ,$$

$$\sigma^o_{zz} = \bar{\sigma}_{z}z = 1250 \text{ lb/in}^2 . \tag{25}$$

For this analysis, the effect of packer-induced stresses are to be considered, and Reference 20 shows that these stresses are dependent upon $P = P_o - P_H$, where P_o is the packer inflation pressure and P_H is the hydraulic fracturing pressure, and are such that

$$\sigma_{\Theta\Theta} = -\frac{Ro^2}{r^2}\sigma_o(\Delta P) , \quad \sigma_{zz} = -0.65\sigma_o(\Delta P)\frac{Ro^2}{r^2} . \tag{26}$$

Superimposing these stresses onto the stresses of Eqs. (B16) to (B21) gives

$$\sigma_{\Theta\Theta} = -\frac{Ro^2}{r^2}(P + \sigma_o(\Delta P)) + 1225(1 + Ro^2/r^2)$$

$$+ 25(1 + 3\,Ro^4/r^4)\cos 2\Theta ,$$

$$\sigma_{zz} = 1250 + 25\frac{Ro^2}{r^2}\cos 2\Theta - 0.65\sigma_o(\Delta P)Ro^2/r^2 ,$$

$$\sigma_{\Theta z} = 350\,(1 + Ro^2/r^2)\cos\Theta , \tag{27}$$

$$\sigma_{rr} = \frac{Ro^2}{r^2}P + 1225(1 - Ro^2/r^2)$$

$$- 25\,(1 - 4\,Ro^2/r^2 + 3\,Ro^4/r^4)\cos 2\Theta ,$$

$$\sigma_{r\Theta} = 25\,(1 + 2\,Ro^2/r^2 - 3\,Ro^4/r^4)\sin 2\Theta ,$$

$$\sigma_{rz} = 350\,(1 - Ro^2/r^2)\sin\Theta ,$$

and on the borehole surface $r = R_o$,

$$\sigma_{\Theta\Theta} = -P - \sigma_o(\Delta P) + 2450 + 100\cos 2\Theta ,$$

$$\sigma_{zz} = 1250 - 0.65\sigma_o(\Delta P) + 25 \cos 2\theta \ , \tag{28}$$

$$\sigma_{\theta z} = 700 \cos \theta \ ,$$

where θ is measured from the vertical axis. The minimum stress on the borehole surface occurs at $\theta = 0$, and for fracture to occur at the measured pressure of $P = 1610$ lb/in^2, the packer-induced stresses must be

$$\sigma_o(\Delta P) = -780 \text{ lb/in}^2 \ . \tag{29}$$

From the analysis of Reference 20, this induced stress level requires $\Delta P \cong 1000$ lb/in^2, which is consistent with the initial packer pressures for this fracture operation as indicated in the data Section IV. In the vertical direction, $\theta = 0$, the stresses of Eq. (27) are

$$\sigma_{\theta\theta} = -2390 \frac{Ro^2}{r^2} + 1225 \ (1 + Ro^2/r^2) + 25(1 + 3 \ Ro^4/r^4) \ ,$$

$$\sigma_{zz} = 1250 - 482 \ Ro^2/r^2 \ ,$$

$$\sigma_{\theta z} = 350 \ (1 + Ro^2/r^2) \ . \tag{30}$$

The angle γ of the maximum stress in the horizontal plane a vertical distance r from the borehole center line is obtained from Eq. (B27), and it is found that

$$\text{Tan } 2\gamma = -1.025 \frac{r^2}{R_o^2} \frac{(1 + Ro^2/r^2)}{(1 - 0.11 \ Ro^2/r^2)} \ , \tag{31}$$

which shows that the angle of the fracture plane twists as the fracture grows away from the borehole. Table 3 shows the theoretical fracture angle as a function of r/R_o and also the observed fracture angle measured during mineback. The observed twist is considerably greater than the theoretical, the fracture actually having broken out of the borehole in a direction essentially parallel to its axis. Measurements of fracture direction at the borehole surface will obviously not indicate far-field fracture-plane orientations.

From Table 3, it is seen that the angle of the fracture γ at the borehole is 33.27° from the axis of the borehole. Assuming that the packer inflation pressure changes with P such that ΔP remains constant and, hence, the packer-induced stresses remain constant, the shut-in pressure, P_{si}, required to just open the crack at the angle γ is obtained from the relation

$$2\sigma_\gamma = -(P_{si} - 2538) - (P_{si} - 1002) \cos 2\gamma - 1400 \sin 2\gamma \ , \tag{32}$$

where σ_γ is now set equal to zero. Solving Eq. (32) for P_{si} with $\gamma = 33.27°$ gives

$$P_{si} = 1182 \text{ lb/in}^2 , \tag{33}$$

which is very close to the observed shut-in pressure for this fracture. Note the effect of both the packer-induced stresses and the angle of fracture γ at the borehole being different from the far-field angle on the shut-in pressure as it relates to the minimum principal stress $\sigma_3 = 900 \text{ lb/in}^2$.

If fracture had initiated at the borehole surface in the direction of the far-field fracture, that is, $\gamma = 45°$, the shut-in pressure from Eq. (43) with $\sigma_\gamma = 0$ at $\gamma = 45°$ gives

$$P_{si}^* = 1138 \text{ lb/in}^2 . \tag{34}$$

The effect of the fluid pressure in the crack makes this analysis quantitatively invalid, and the actual shut-in pressure will be close to the minimum in-situ stress σ_3, that is, $P_{si} = 900 \text{ lb/in}^2$. But, qualitatively, because the direction of fracture at the borehole is not normal to σ_3, a measured shut-in pressure which is higher than σ_3 will result, that is, the fracture will close at the borehole at a higher pressure than that required to keep the fracture open in the far field. Comparison of Eqs. (33) and (34) indicate that, for this example, the difference in pressure is $P_{si} - P_{si}^* = 44 \text{ lb/in}^2$, and a measured shut-in pressure of $P_{si} = 944 \text{ lb/in}^2$ rather than the 900 lb/in^2 associated with σ_3 would be expected.

Table 3

Angle of Minimum Stress γ with Distance r/R_o from the Borehole

r/R_o	Theoretical γ Eq. (31)	Measured γ Fig. 11
1.0	33.3°	
1.5	37.0°	
2.0	39.6°	5°
2.5	41.2°	
3.0	42.2°	
3.25	42.6°	(13°)*
3.5	42.9°	10°
4.0	43.4°	
5.0	43.9°	10°
5.25	44.0°	(30°)*
11.5	44.8°	20°
∞	45.0°	45°

* ( ) Indicates measurements made below the borehole.

Summary

This report describes the activities in G Tunnel, NTS, which have been involved with estimating in-situ stresses from hydrofrac measurements. Following a description of the field-test equipment and procedures, selected data are presented which are considered to be representative of the more than 100 fracturing operations conducted to date. Estimates of the in-situ stresses are then obtained by using this selected data and theoretical analysis. Data from other hydraulically fractured boreholes in G Tunnel are similarly analyzed and included as a part of this summary.

Figure 13 shows the dips of induced fractures on a vertical section through the G Tunnel. Under the cap of the mesa, the fracture planes are within 5° of vertical. Toward the edge of the mesa, the fractures begin to tilt. Beneath the mesa edge, the HF 47 fracture is tilted 30° from vertical. The tilt of the fractures continues to increase farther under the sloping portion of the mesa, suggesting that the tilt is related to topography.

Figure 14 shows the azimuths of the fractures plotted on a map of G Tunnel. (The long dashed line with the two bends shows the location of the vertical section shown in Figure 13.) Under the mesa cap, azimuths range from N35°E to N60°E, and, under the mesa edge, about N30°E. The two fractures under the sloping portion show azimuths of N12°E and N, that of the N fracture being a calculated value. In this region the fractures appear parallel with contour lines.

Thus, we see reasonably consistent behavior of fracture planes and the direction of minimum in-situ stress which is normal to the planes. The figures show vertical fractures under 1400 feet of overburden with a level surface, as well as tilted fractures under a sloping surface with azimuths that parallel contour lines on the sloping surface.

In-situ stresses have been estimated for one point in G Tunnel by using an overcoring technique. Table 4 shows the overcore results compared with those of HFS 13, 14 and 15 that lie 150 feet west and HF 30 that lies 50 feet east of the overcore (Figure 14); details of the overcore operation are presented in Reference 22.

Table 4

Overcore and Hydrofrac Tests Compared

In-Situ Stress (Orientation)	Overcore		HFS 13-15		HF 30	
	Magnitude (lb/in^2)	Orient.	Magnitude (lb/in^2)	Orient.	Magnitude (lb/in^2)	Orient.
Minimum (Horiz.)	374	N68°W; 7° below Horiz.	450	N52°W	410	N51°W; 7° below Horiz.
Maximum (Horiz.)	1233	N22°E	1080	N38°E	---	N40°E
(Vertical)	986	7° from Vert. N83°W	1194	Vert.	915	7° from Vert. N51°W

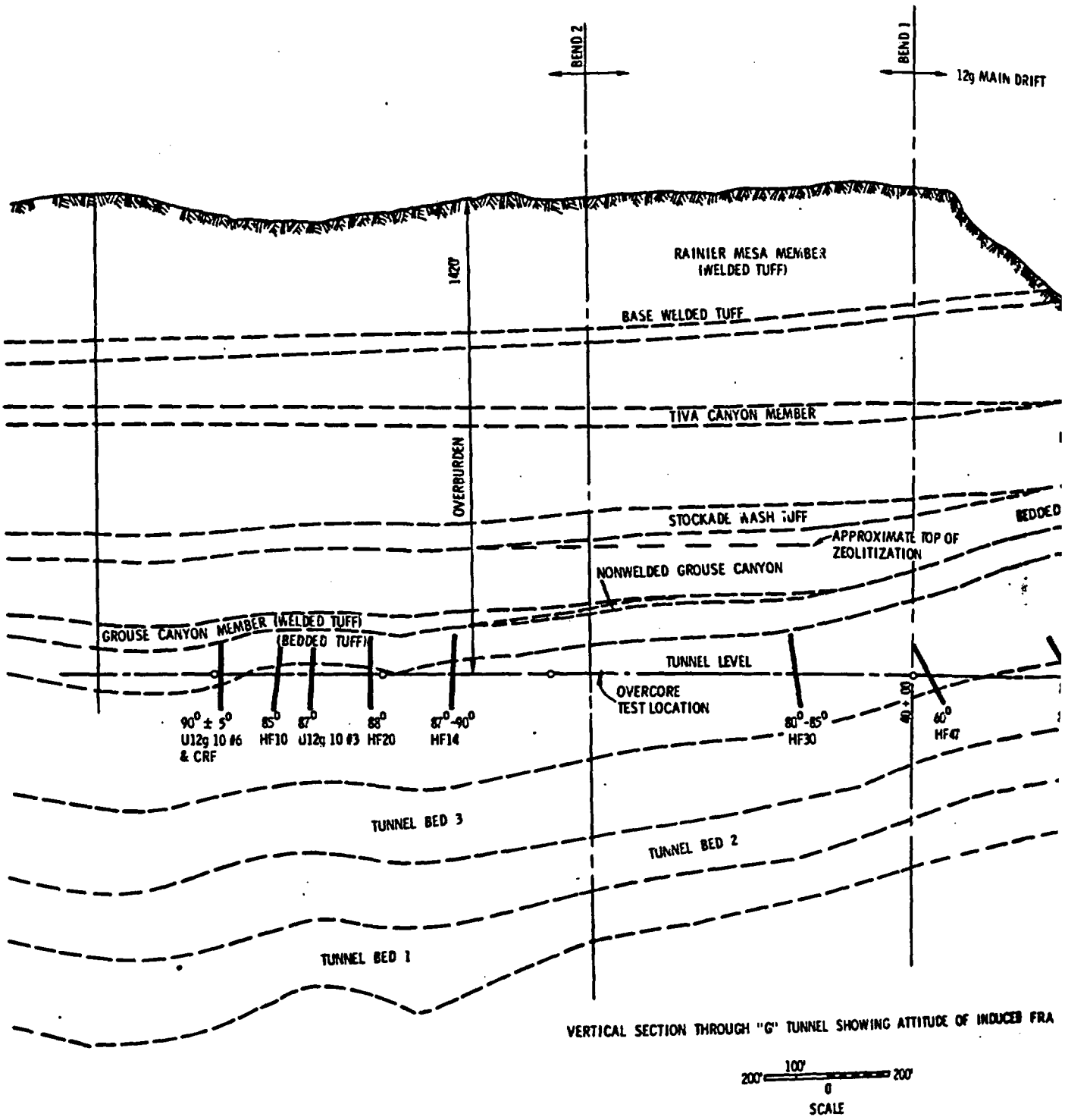

Figure 13. Vertical Section through G T

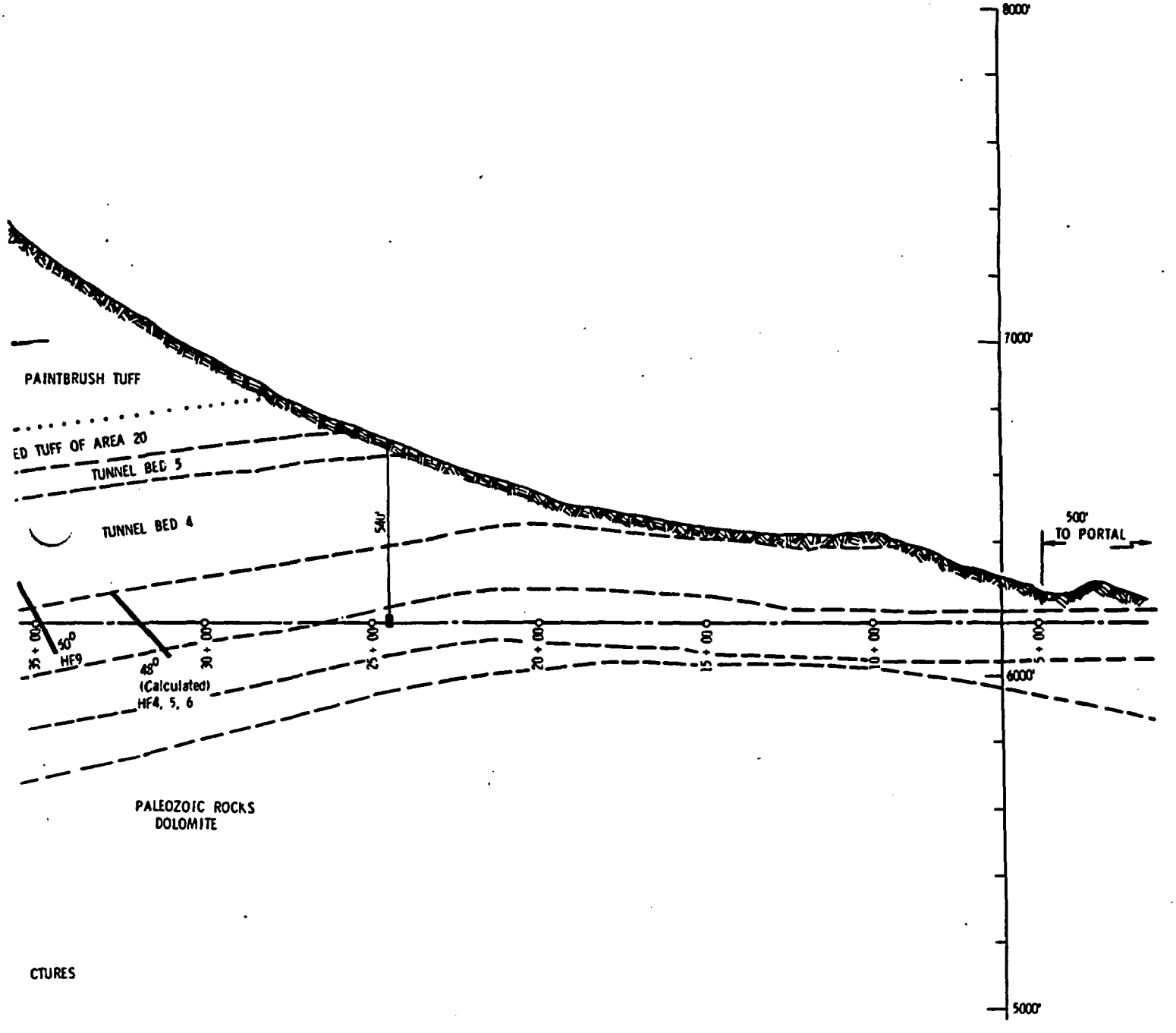

u 1, Showing Direction of Induced Fractures

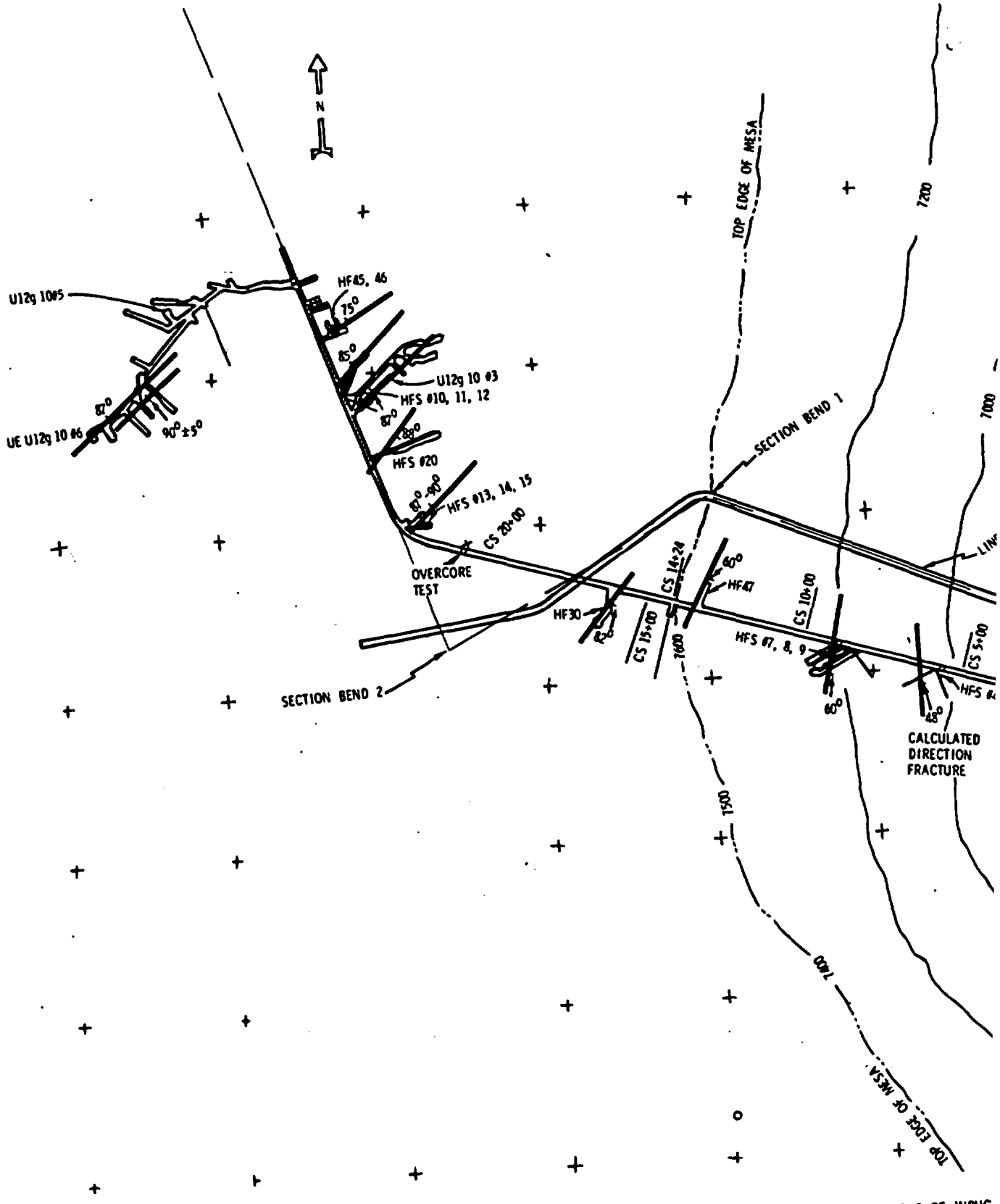

PLAN MAP OF "G" TUNNEL SHOWING AZIMUTHS OF INDUC

Figure 14. G Tunnel Ma

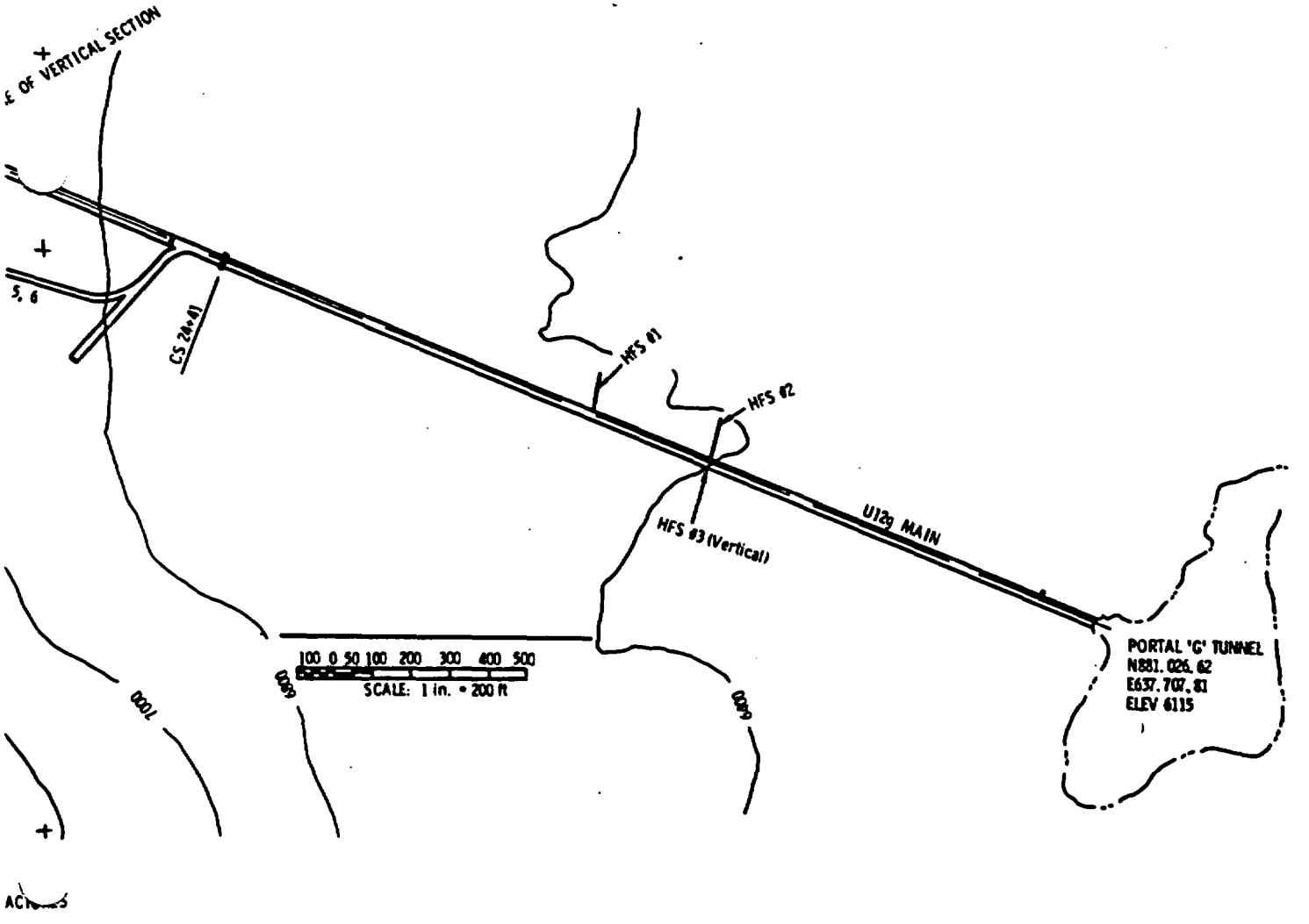

howing Azimuths of Induced Fractures

Table 4 shows that the values of the minimum stresses agree reasonably well and all are horizontal. The maximum horizontal and vertical values in all cases except HF 30 differ by only 200 lb/in^2. The azimuths of all horizontal stresses differ by about 20°, and those of vertical stress are within 7° of vertical. Despite the uncertainties of obtaining in-situ stress values from hydrofracturing and the uncertainties of overcoring caused by strain measurements and variations in elastic moduli and in Poisson's ratio, reasonable agreement between the two techniques is found.

As a final part of this summary, certain problems in estimating in-situ stresses from hydrofrac pressure data will be pointed out. These problems have been encountered during field operations and while analyzing data from over 100 fracturing operations in G Tunnel. Some of these have been mentioned in detail elsewhere in this report and are repeated here for emphasis.

First, the inverse problem of obtaining principal stress magnitudes and directions from hydrofrac tests on cylindrical boreholes poses formidable difficulties, not the least being that the stress field is not unique. On the other hand, hydrofrac does offer the possibility of obtaining at least two pieces of information, not directly measurable by other methods, with great accuracy: the <u>magnitude</u> and the <u>direction</u> of the minimum principal stress. The magnitude of the minimum stress is approximately equal to the instantaneous shut-in pressure (P_{si}), that is, the pressure the hydrofrac system drops to immediately after the pumps are shut off (Figure 2). Theoretically, P_{si} is slightly greater than the magnitude of the minimum principal stress, this difference usually being small, increasing as the angle of the fracture plane increases with respect to the borehole axis. But in a number of cases, a well-defined P_{si} was not observed, and the pressure continued to drop essentially exponentially after the pump was shut down. The reasons for this behavior are not clear. Perhaps, if a fixed percentage of the stabilized flow-pressure (P_f) is used, a reasonably accurate estimate of the P_{si} under these conditions could be made, but this idea must be more thoroughly studied. If the problem is primarily absorption of the fluid into the rock--not likely in the ash-fall tuff environment of G Tunnel--chemical additives to the fracturing fluid might retard absorption long enough for a definite P_{si} to be obtained. In short, inability to measure P_{si} effectively eliminates one of the two important pieces of information that can be obtained from hydrofrac pressure records.

Hydrofracturing creates a crack which eventually propagates in a plane that is perpendicular to the minimum principal stress. This is the second observable or measurable quantity unique to hydrofrac methods for estimating in-situ stresses, that is, the <u>direction</u> of the minimum principal stress. Unfortunately, unless the axis of the cylindrical borehole lies in the fracture plane, the direction of fracture at the borehole may not be the same as the direction in the far field. (Daneshy[24] also discusses this effect.) This effect was detailed in the results section where the fracture was mapped after mineback, showing that the fracture twisted as it left the borehole surface. Observation of the fractured borehole after a test, either with impression packers or down-hole cameras, may reveal a fracture plane that has no relation to that of the far-field fracture. In effect,

the cylindrical borehole itself introduces a geometrical bias into any effort to determine the far-field fracture plane. To circumvent this geometrical complication, the idea of hydrofracing a spherical cavity, which has no orientation bias, has been advanced.[19] Analysis shows that the spherical cavity will fracture along a plane perpendicular to that of the minimum principal stress, and post-fracture examination will determine the orientation of this plane. The P_{si} will determine the magnitude of this minimum principal stress, and the P_c provides a relation between the magnitudes of the two other principal stresses which lie in the fracture plane. Other advantages of hydrofracing spherical cavities are detailed in Reference 19.

Other methods for determining the far-field fracture plane should be explored since knowing the orientation of this plane is crucial for estimating in-situ stresses. The orientations of most fracture planes in G Tunnel have been determined by minebacking around the fractured borehole. This method is not only extremely expensive but physically impossible under most practical conditions.

Another significant problem is the effect that packer-induced stresses have on the borehole. These stresses have been analyzed by W. E. Warren[20] who shows that, for a given packer, these induced stresses depend on the difference between packer and hydrofrac pressures and can be significant. To minimize packer-induced stresses, this pressure difference should be kept as low as possible during the entire fracturing operation. These packer-induced stresses are localized around the packer at the borehole and will have negligible effect on measured P_{si} values and on orientation of the fracture plane in the far field. However, the breakdown pressure (P_c), which provides additional information about the in-situ stress field may be considerably affected by packer-induced stresses. For a given in-situ stress field, ignoring the packer-induced stresses leads to a higher predicted P_c than will actually be necessary to initiate fracture. Working backwards, the measured P_c will not give an accurate relationship between the existing in-situ stresses.

The importance of these packer-induced stresses seems quite evident from observations made during mineback of the fractures in G Tunnel. A number of the fractures initiated at or near the packer. To account accurately for packer-induced stresses in the analysis, the pressure in the packer should be recorded during fracturing, at least up to the time breakdown of the formation occurs.

Finally, there is the problem of determining the effective tensile strength of the formation under conditions of a pressurized borehole. The tensile strength of brittle materials is strongly dependent upon the distribution of flaws and imperfections in the material which create stress concentrations and enhance fracture initiation and growth. Under the conditions of a uniaxial tension test, the entire specimen is subjected to a uniform tensile stress so that flaws and imperfections throughout the entire test specimen become candidates for fracture initiation points. Thus, the tensile strength obtained from a uniaxial tensile test is a measure of the strength of the weakest point anywhere in the entire specimen. On the other hand, the stress field associated with a pressurized cylindrical borehole

exhibits maximum tension at the borehole surface and decreases rapidly with distance into the material. Thus, only those flaws and imperfections in a narrow region around the borehole are subjected to the maximum tensile stress, and the stress levels required to initiate fracture at the borehole can be expected to be considerably higher than the stress levels required to initiate fracture in the uniaxial tensile test. For Coeur d'Alene Revett Quartzite, Haimson[21] finds the effective tensile strength at a pressurized borehole to be about 2 or 3 times the uniaxial tensile strength. In this report, an effective tensile strength of T = 300 psi is used, which is about twice the uniaxial tensile strength as listed in Table 2. This value of T has not been experimentally verified. Hydrofracing a spherical cavity rather than a cylindrical borehole,[19] with subsequent repressurization after initial fracturing, offers a direct measurement of the effective tensile strength of the formation under this loading condition.

References

[1] L. D. Tyler and W. C. Vollendorf, "Physical Observations and Mapping of Cracks Resulting from Hydraulic Fracturing In-Situ Stress measurements," Soc Pet Eng AIME Paper No. SPE-5542 (1975).

[2] J. B. Clark, "A Hydraulic Process for Increasing the Productivity of Wells," Trans AIME, 186:1-8 (1949).

[3] M. K. Hubert and D. G. Willis, "Mechanics of Hydraulic Fracturing," Trans AIME, 210:153-66 (1957).

[4] A. E. Scheidegger, "Stresses in Earth's Crust as Determined from Hydraulic Fracturing Data," Geologic und Bauwesen, 27:45 (1962).

[5] R. O. Kehle, "The Determination of Tectonic Stresses Through Analysis of Hydraulic Well Fracturing," J Geophysical Res, 69(2):259-73 (1964).

[6] C. Fairhurst, "Measurement of In-Situ Rock Stresses, with Particular Reference to Hydraulic Fracturing," Rock Mechanics & Engineering Geo, 2(3-4):129-47 (1964).

[7] B. C. Haimson, "Hydraulic Fracturing in Porous and Nonporous Rock and Its Potential for Determining In-Situ Stresses at Great Depth" (PhD Thesis, U of Minn, July 1968).

[8] B. C. Haimson and C. Fairhurst, "Hydraulic Fracturing in Porous-Permeable Materials," J Pet Tech, 21(7):811-17 (July 1969).

[9] B. C. Haimson, "Earthquake Related Stresses at Rangely, Colorado," New Horizons in Rock Mechanics, ed H. Hardy & R. Stefanko (New York: Am Soc C E, 1973), pp 689-708.

[10] C. B. Raleigh, J. H. Healy, and J. D. Bredehoeft, "An Experiment in Earthquake Control at Rangely, Colorado," Science, 191:1230-37 (1976).

[11] W. S. Keys et al, "In-Situ Stress Measurements Near the San Andreas Fault in Central California," J Geophys Res 84(B4):1583-91 (1979).

[12] A. S. Abou-Sayed, C. E. Brechtel, and R. J. Clifton, "In-Situ Stress Determination by Hydrofracturing: A Fracture Mechanics Approach," J Geophys Res 83:2851-62 (June 1978).

[13] G. C. Howard and C. R. Fast "Hydraulic Fracturing," Soc Pet Eng, (1970). A monograph.

[14] R. L. Aamodt, An Experimental Measurement of In-Situ Stress in Granite by Hydraulic Fracturing, LA-5605-MS (Los Alamos: Los Alamos Scientific Laboratory, NM, April 1974).

[15] C. H. Miller, A Method for Stress Determination in N, E, and T Tunnels, NTS, by Hydraulic Fracturing with Comparison of Overcoring Methods, USGS474-222 (Washington, DC: The US Geological Survey, May 1976).

[16] B. C. Haimson et al, Deep Stress Measurements in Tuff at the Nevada Test Site, TR 74-11 (Salt Lake City: Terra Tek, Inc., 1974).

[17] L. Obert, In-Situ Stresses in Rock, Ranier Mesa, Nevada Test Site, WT-1869 (College Park, MD: U.S. Bureau of Mines, Applied Physics Laboratory, Sept. 1964).

[18] C. H. Miller et al, Determination of In-Situ Stress at U12C.18 Working Point, Rainier Mesa, Nevada Test Site, USGS-474-217 (Washington, DC: U.S. Geological Survey, Dec. 1975). Area Report 12-42.

[19] W. E. Warren, Determination of In-Situ Stresses from Hydraulically Fractured Spherical Cavities, SAND78-1832 (Albuquerque: Sandia Laboratories, 1978).

[20] W. E. Warren, Packer Induced Stresses During Hydraulic Well Fracturing, SAND79-1986 (Albuquerque: Sandia Laboratories, Dec. 1979).

[21] B. C. Haimson, Determination of In-Situ Stresses Around Underground Excavations by Means of Hydraulic Fracturing (Madison: University of Wisconsin, Engineering Experiment Station, April 1974). Final Tech Report, Contract No. H0220080.

[22] W. L. Ellis and J. R. Ege, Determination of In-Situ Stress in U12g Tunnel, Rainier Mesa, Nevada Test Site, Nevada, USGS-474-219 (Washington, DC: U.S. Geological Survey, Dec. 1976). Area Report 12-37.

[23] Unpublished memo from Warren to Smith.

[24] A. A. Daneshy, "A Study of Inclined Hydraulic Fractures," Soc. Pet. Eng. J, 13(2):61-68 (1973).

APPENDIX A

Hydrofrac Hole List (U12G)

Name	Fractured	Mineback	Location or Associated Work
HFS 1	Yes	No	Horizontal hole at CS 1400 M.D.
HFS 2	Yes	No	Horizontal hole at CS 1060 M.D.
HFS 3	Yes	No	Vertical hole at CS 1060 M.D.
HFS 4	Yes	No	Series of 2 horizontal (5&6) and one vertical (4) holes at CS 580 M.D.B.P.
HFS 5	Yes	No	
HFS 6	Yes	No	
HFS 7	Yes	No	Series of 2 horizontal (8&9) and one vertical (7) holes at CS 8 + 50 M.D.B.P.
HFS 8	Yes	No	
HFS 9	Yes	Yes	
HFS 10	Yes	Yes	Series of 2 horizontal (10&11) and one vertical (12) holes at CS 27 + 38 M.D.B.P.
HFS 11	Yes	No	
HFS 12	Yes	No	
HFS 13	Yes	No	CS 22 + 38 - Series of 3 holes at bend in M.D.B.P. - 13 and 14 horizontal, 15 vertical
HFS 14	Yes	Yes	
HFS 15	Yes	Yes	
HFS 16	No	No	CS 28 + 34 M.D.B.P.
HFS 17	Yes	Yes	CS 31 + 27 M.D.B.P.
HFS 18	Yes	Yes	CS 30 + 30 M.D.B.P.
HFS 19	Yes	Yes	CS 29 + 28 M.D.B.P.
HF 20	Yes	Oct 77	CS 25 + 20 M.D.B.P.
HFS 21	No	No	CS 31 + 60 M.D.B.P.
HFS 22	No	No	CS 31 + 60 M.D.B.P.
HFS 23	Dec 77	Jan 78	CS 3 + 66 VDH #5 Eval. Drift
EV 5-2	Jan 78	Feb 78	CS 2 + 30 VDH #5 Eval. Drift
HFS 24	Summer 77	Summer 77	Collar in Eval. Drift No. 3 Associated with Puff 'n Tuff Ex
HFS 25	Summer 77	No	Collar in EFH No. 2
HFS 26/27/28			Unassigned names
HFS 29	Feb 79	No	CS 14 + 24 M.D.B.P.
HFS 30	Oct 78/ Feb 79	Fall 79	CS 16 + 15 M.D.B.P. Now GSAC Test Area
HFS 31	Aug 77	?	In Ev #10 Drift - Now Multifrac Test Area
HF 32	March 78	No	Holes in right rib of Puff 'n Tuff Drift - Associated with RS 1 & 2
HF 33	March 78	Summer 78	
HF 34	March 78	No	
HF 35	March 78	Summer 78	
HF 36	--	--	
HF 37	June 78	Fall 78	Puff 'n Tuff Drift -- Associated with RS4
HF 38	June 78	Fall 78	
HF 39	Sept 78	No	Right Rib of HFS 20 Drift

Hydrofrac Hole List (U12G)

Name	Fractured	Mineback	Location or Associated Work	
HF 40 HF 41/42	Sept 78	No	Frac Hole Geophone Holes	Seismic/Hydrofrac Experiment in HFS 20 Drift
HF 43/44			Geophone Holes	Drift
HF 45	Sept 78	Oct 78	Associated with RS5	Hole collars in
HF 46	Sept 78	Oct 78	Associated with RS6	HFS 19 Drift
HF 47	Feb 80	March 80	In DNEX Alcove at CS 13 + 50 M.D.B.P.	

APPENDIX B

Complete Stress and Displacement Fields

For completeness of the analysis of this report, stress and displacement fields around an infinitely-long cylindrical cavity imbedded in an infinite, linearly-elastic media are calculated in this Appendix. The cavity is subjected to a uniform pressure P along its entire length and a uniform stress system exists in the far field. Classical linear elasticity theory is used, defining displacements in the usual way, tensile stresses being positive. A simple change of sign in the stress tensor then gives results in the form needed in the body of this report for determining in-situ stresses.

In a Cartesian coordinate system (x,y,z), the uniform stress field is obtained from the displacement field

$$2\mu\ u_x = \frac{(\sigma^o_{xx} - \nu\sigma^o_{yy} - \nu\sigma^o_{zz})}{(1+\nu)}\ x + \sigma^o_{xy}\ y + \sigma^o_{xz}\ z$$

$$2\mu\ u_y = \sigma^o_{xy}\ x + \frac{(\sigma^o_{yy} - \nu\sigma^o_{xx} - \nu\sigma^o_{zz})}{(1+\nu)}\ y + \sigma^o_{yz}\ z$$

$$2\mu\ u_z = \sigma^o_{xz}\ x + \sigma^o_{yz}\ y + \frac{(\sigma^o_{zz} - \nu\sigma^o_{xx} - \nu\sigma^o_{yy})}{(1+\nu)}\ z\ , \qquad \text{(B1)}$$

where μ, ν are the material shear modulus and Poisson's ratio, respectively. With dilatation $\Delta = \frac{\partial u_x}{\partial x} + \frac{\partial u_y}{\partial y} + \frac{\partial u_z}{\partial z}$ given by

$$2\mu\ \Delta = \frac{(1-2\nu)}{(1+\nu)}\ (\sigma^o_{xx} + \sigma^o_{yy} + \sigma^o_{zz})\ , \qquad \text{(B2)}$$

this displacement field gives the uniform stress field

$$\sigma_{xx} = \sigma^o_{xx}\ ,\ \sigma_{yy} = \sigma^o_{yy}\ ,\ \sigma_{zz} = \sigma^o_{zz}$$

$$\sigma_{xz} = \sigma^o_{xz} \quad \sigma_{yz} = \sigma^o_{yz} \quad \sigma_{xy} = \sigma^o_{xy}\ . \qquad \text{(B3)}$$

In cylindrical coordinates (r,θ,z),

$$u_r = \cos\theta\ u_x + \sin\theta\ u_y$$

$$u_\theta = -\sin\theta\ u_x + \cos\theta\ u_y$$

$$u_z = u_z\ , \qquad \text{(B4)}$$

the cylindrical components of the displacement field (B1), using (B4), become

$$2\mu\ u_r = \sigma^o_{xx}\ r\cos^2\theta + \sigma^o_{yy}\ r\sin^2\theta + 2\sigma^o_{xy}\ r\cos\theta\sin\theta$$

$$- \frac{\nu}{(1+\nu)}(\sigma^o_{xx} + \sigma^o_{yy} + \sigma^o_{zz})r + (\sigma^o_{xz}\cos\theta + \sigma^o_{yz}\sin\theta)z$$

$$2\mu\ u_\theta = -(\sigma^o_{xx} - \sigma^o_{yy})r\cos\theta\sin\theta + \sigma^o_{xy}\ r(\cos^2\theta - \sin^2\theta)$$

$$- (\sigma^o_{xz}\sin\theta - \sigma^o_{yz}\cos\theta)z$$

$$2\mu\ u_z = (\sigma^o_{xz}\cos\theta + \sigma^o_{yz}\sin\theta)r + \frac{(\sigma^o_{zz} - \nu\sigma^o_{xx} - \nu\sigma^o_{yy})}{(1+\nu)}\ z\ , \qquad \text{(B5)}$$

and the cylindrical components of stress become

$$\sigma_{rr} = \sigma^o_{xx}\cos^2\theta + \sigma^o_{yy}\sin^2\theta + 2\sigma^o_{xy}\cos\theta\sin\theta$$

$$\sigma_{\theta\theta} = \sigma^o_{xx}\sin^2\theta + \sigma^o_{yy}\cos^2\theta - 2\sigma^o_{xy}\cos\theta\sin\theta$$

$$\sigma_{zz} = \sigma^o_{zz}$$

$$\sigma_{\theta z} = -(\sigma^o_{xz}\sin\theta - \sigma^o_{yz}\cos\theta)$$

$$\sigma_{rz} = \sigma^o_{xy}\cos\theta + \sigma^o_{yz}\sin\theta$$

$$\sigma_{r\theta} = -(\sigma^o_{xx} - \sigma^o_{yy})\cos\theta\sin\theta + \sigma^o_{xy}(\cos^2\theta - \sin^2\theta)\ . \qquad \text{(B6)}$$

This stress field can be readily shown to satisfy the equilibrium equations.[B1]

On the surface of the infinitely-long cylindrical borehole defined by $r = R_o$, the boundary stresses are prescribed as

$$\sigma_{rr} = -P\ ,\ \sigma_{rz} = \sigma_{r\theta} = 0\ ,\ \text{on } r = R_o \qquad \text{(B7)}$$

where P is the applied borehole pressure. Stress and displacement fields vanishing at $r \to \infty$ will now be obtained, which, when superimposed with the uniform stress field of Eq. (B6) satisfy the conditions of Eq. (B7). Consider the antiplane displacement field

$$u_r = 0\ ,\ u_\theta = 0\ ,\ u_z = W(r,\theta)\ . \qquad \text{(B8)}$$

The stress field is

$$\sigma_{rr} = 0 \ , \ \sigma_{\theta\theta} = 0 \ , \ \sigma_{zz} = 0 \ , \ \sigma_{r\theta} = 0$$

$$\frac{1}{\mu}\,\sigma_{\theta z} = \frac{1}{r}\frac{\partial W}{\partial \theta}, \ \frac{1}{\mu}\sigma_{rz} = \frac{\partial W}{\partial r} \ . \tag{B9}$$

This stress field satisfies equilibrium if

$$\frac{1}{r}\frac{\partial}{\partial r}\left(r\,\frac{\partial W}{\partial r}\right) + \frac{1}{r^2}\frac{\partial^2 W}{\partial \theta^2} = \nabla^2 W = 0. \tag{B10}$$

Now take

$$W = \frac{R_o^2}{\mu r}\,(\sigma_{xz}^o \ \cos\theta + \sigma_{yz}^o \sin\theta) \tag{B11}$$

in Eq. (B9) to get

$$2\mu\ u_z = \frac{2R_o^2}{r}\,(\sigma_{xz}^o \cos\theta + \sigma_{yz}^o \sin\theta) \ ,$$

$$\sigma_{\theta z} = -\frac{R_o^2}{r^2}\ (\sigma_{xz}^o \sin\theta - \sigma_{yz}^o \cos\theta) \ ,$$

$$\sigma_{rz} = -\frac{R_o^2}{r^2}\,(\sigma_{xz}^o \cos\theta + \sigma_{yz}^o \sin\theta) \ . \tag{B12}$$

This stress field vanishes for large r like r^{-2}, and on $r = R_o$, annihilates the σ_{rz} stress from the uniform stress field of Eq. (B6).

To eliminate the cylindrical surface stresses σ_{rr} and $\sigma_{r\theta}$ at the surface $R = R_o$ and apply the uniform pressure $\sigma_{rr} = -P$ on this surface, use is made of the plane strain solution

$$2\mu\ u_r = \frac{R_o^2}{r}\left[P + \frac{1}{2}\,(\sigma_{xx}^o + \sigma_{yy}^o)\right]$$

$$+ \left[4(1-\nu)\,\frac{R_o^2}{r} - \frac{R_o^4}{r^3}\right]\left[\frac{1}{2}\,(\sigma_{xx}^o - \sigma_{yy}^o)\cos 2\theta + \sigma_{xy}^o \sin 2\theta\right]$$

$$2\mu\ u_\theta = -\left[2(1-2\nu)\,\frac{R_o^2}{r} + \frac{R_o^4}{r^3}\right]\left[\frac{1}{2}\,(\sigma_{xx}^o - \sigma_{yy}^o)\sin 2\theta - \sigma_{xy}^o \cos 2\theta\right]$$

$$2\mu\ u_z = 0 \ . \tag{B13}$$

With the dilatation Δ given by

$$2\mu\ \Delta = -4(1 - 2\nu)\ \frac{R_o^2}{r^2}\left[\frac{1}{2}\ (\sigma_{xx}^o - \sigma_{yy}^o)\cos 2\theta + \sigma_{xy}^o \sin 2\theta\right] , \qquad \text{(B14)}$$

the stresses associated with this displacement are given by

$$\sigma_{rr} = -\frac{R_o^2}{r^2}\left[P + \frac{1}{2}\ (\sigma_{xx}^o + \sigma_{yy}^o)\right]$$

$$- \left[4\ \frac{R_o^2}{r^2} - 3\ \frac{R_o^4}{r^4}\right]\left[\frac{1}{2}\ (\sigma_{xx}^o - \sigma_{yy}^o)\cos 2\theta + \sigma_{xy}^o \sin 2\theta\right]$$

$$\sigma_{\theta\theta} = \frac{R_o^2}{r^2}\left[P + \frac{1}{2}\ (\sigma_{xx}^o + \sigma_{yy}^o)\right]$$

$$- 3\ \frac{R_o^4}{r^4}\left[\frac{1}{2}\ (\sigma_{xx}^o - \sigma_{yy}^o)\cos 2\theta + \sigma_{xy}^o \sin 2\theta\right]$$

$$\sigma_{zz} = -4\nu\ \frac{R_o^2}{r^2}\left[\frac{1}{2}\ (\sigma_{xx}^o - \sigma_{yy}^o)\cos 2\theta + \sigma_{xy}^o \sin 2\theta\right]$$

$$\sigma_{r\theta} = -\left[2\ \frac{R_o^2}{r^2} - 3\ \frac{R_o^4}{r^4}\right]\left[\frac{1}{2}\ (\sigma_{xx}^o - \sigma_{yy}^o)\sin 2\theta - \sigma_{xy}^o \cos 2\theta\right]$$

$$\sigma_{\theta z} = \sigma_{rz} = 0\ . \qquad \text{(B15)}$$

This stress field vanishes for large r like r^{-2} and hence has no effect at infinity on the uniform stress field. This stress field satisfies the equilibrium equations of Reference B1. The total stresses from the uniform field of Eq. (B6) and the two solutions used to satisfy boundary conditions on $r = R_o$ given by Eqs. (B12) and (B15) become

$$\sigma_{\theta\theta} = \frac{R_o^2}{r^2}\ P + \frac{1}{2}\ (\sigma_{xx}^o + \sigma_{yy}^o)\left(1 + \frac{R_o^2}{r^2}\right)$$

$$- \left(1 + 3\ \frac{R_o^4}{r^4}\right)\left[\frac{1}{2}\ (\sigma_{xx}^o - \sigma_{yy}^o)\cos 2\theta + \sigma_{xy}^o \sin 2\theta\right] , \qquad \text{(B16)}$$

$$\sigma_{zz} = \sigma_{zz}^o - 4\nu\ \frac{R_o^2}{r^2}\left[\frac{1}{2}\ (\sigma_{xx}^o - \sigma_{yy}^o)\cos 2\theta + \sigma_{xy}^o \sin 2\theta\right] , \qquad \text{(B17)}$$

$$\sigma_{\theta z} = -(\sigma_{xz}^o \sin\theta - \sigma_{yz}^o \cos\theta)\left(1 + \frac{R_o^2}{r^2}\right) , \qquad \text{(B18)}$$

$$\sigma_{rr} = -\frac{R_o^2}{r^2} P + \frac{1}{2}\left(1 - \frac{R_o^2}{r^2}\right)(\sigma_{xx}^o + \sigma_{yy}^o)$$

$$+ \left(1 - 4\frac{R_o^2}{r^2} + 3\frac{R_o^4}{r^4}\right)\left[\frac{1}{2}(\sigma_{xx}^o - \sigma_{yy}^o)\cos 2\theta + \sigma_{xy}^o \sin 2\theta\right] , \quad \text{(B19)}$$

$$\sigma_{r\theta} = -\left(1 + 2\frac{R_o^2}{r^2} - 3\frac{R_o^4}{r^4}\right)\left[\frac{1}{2}(\sigma_{xx}^o - \sigma_{yy}^o)\sin 2\theta - \sigma_{xy}^o \cos 2\theta\right] \quad \text{(B20)}$$

$$\sigma_{rz} = \left(1 - \frac{R_o^2}{r^2}\right)(\sigma_{xz}^o \cos\theta + \sigma_{yz}^o \sin\theta) . \quad \text{(B21)}$$

These stress results have also been obtained by Leeman.[B2] The total displacement field is the sum of the displacement fields given by Eqs. (B5), (B12), and (B13). These displacements are

$$2\mu \frac{u_r}{R_o} = P\frac{R_o}{r} + \frac{1}{2}(\sigma_{xx}^o + \sigma_{yy}^o)\left(\frac{r}{R_o} + \frac{R_o}{r}\right) - \frac{\nu}{(1+\nu)}(\sigma_{xx}^o + \sigma_{yy}^o + \sigma_{zz}^o)\frac{r}{R_o}$$

$$+ \left[\frac{r}{R_o} + 4(1-\nu)\frac{R_o}{r} - \frac{R_o^3}{r^3}\right]\left[\frac{1}{2}(\sigma_{xx}^o - \sigma_{yy}^o)\cos 2\theta + \sigma_{xy}^o \sin 2\theta\right]$$

$$+ (\sigma_{xz}^o \cos\theta + \sigma_{yz}^o \sin\theta)\frac{z}{R_o} \quad \text{(B22)}$$

$$2\mu \frac{u_\theta}{R_o} = -\left[\frac{r}{R_o} + 2(1-2\nu)\frac{R_o}{r} + \frac{R_o^3}{r^3}\right]\left[\frac{1}{2}(\sigma_{xx}^o - \sigma_{yy}^o)\sin 2\theta - \sigma_{xy}^o \cos 2\theta\right]$$

$$- (\sigma_{xz}^o \sin\theta - \sigma_{yz}^o \cos\theta)\frac{z}{R_o} \quad \text{(B23)}$$

$$2\mu \frac{u_z}{R_o} = (\sigma_{xz}^o \cos\theta + \sigma_{yz}^o \sin\theta)\left(\frac{r}{R_o} + 2\frac{R_o}{r}\right) + \frac{(\sigma_{zz}^o - \nu\sigma_{xx}^o - \nu\sigma_{yy}^o)}{(1+\nu)}\frac{z}{R_o} . \quad \text{(B24)}$$

The nonzero stresses on the surface of the borehole $r = R_o$ are

$$\sigma_{\theta\theta} = P + \sigma_{xx}^o + \sigma_{yy}^o - 4\left[\frac{1}{2}(\sigma_{xx}^o - \sigma_{yy}^o)\cos 2\theta + \sigma_{xy}^o \sin 2\theta\right]$$

$$\sigma_{zz} = \sigma_{zz}^o - 4\nu\left[\frac{1}{2}(\sigma_{xx}^o - \sigma_{yy}^o)\cos 2\theta + \sigma_{xy}^o \sin 2\theta\right]$$

$$\sigma_{\theta z} = -2(\sigma_{xz}^o \sin\theta - \sigma_{yz}^o \cos\theta)$$

$$\sigma_{rr} = -P . \quad \text{(B25)}$$

The plane element at the borehole surface is shown in Figure B1. The stresses on the face inclined an angle γ measured from the z axis are given by

$$\sigma_\gamma = \frac{1}{2}(\sigma_{\theta\theta} + \sigma_{zz}) + \frac{1}{2}(\sigma_{\theta\theta} - \sigma_{zz})\cos 2\gamma + \sigma_{\theta z} \sin 2\gamma$$

$$\tau_\gamma = -\frac{1}{2}(\sigma_{\theta\theta} - \sigma_{zz})\sin 2\gamma + \sigma_{\theta z}\cos 2\gamma \ . \tag{B26}$$

The normal stress σ_γ maximizes or minimizes at the angle

$$\tan 2\gamma = \frac{2\sigma_{\theta z}}{(\sigma_{\theta\theta} - \sigma_{zz})} \ , \tag{B27}$$

and the maximum or minimum values of σ_γ are given by

$$\sigma_{\substack{max\\min}} = \frac{1}{2}(\sigma_{\theta\theta} + \sigma_{zz}) \pm \sqrt{\frac{1}{4}(\sigma_{\theta\theta} - \sigma_{zz})^2 + \sigma_{\theta z}^2} \ . \tag{B28}$$

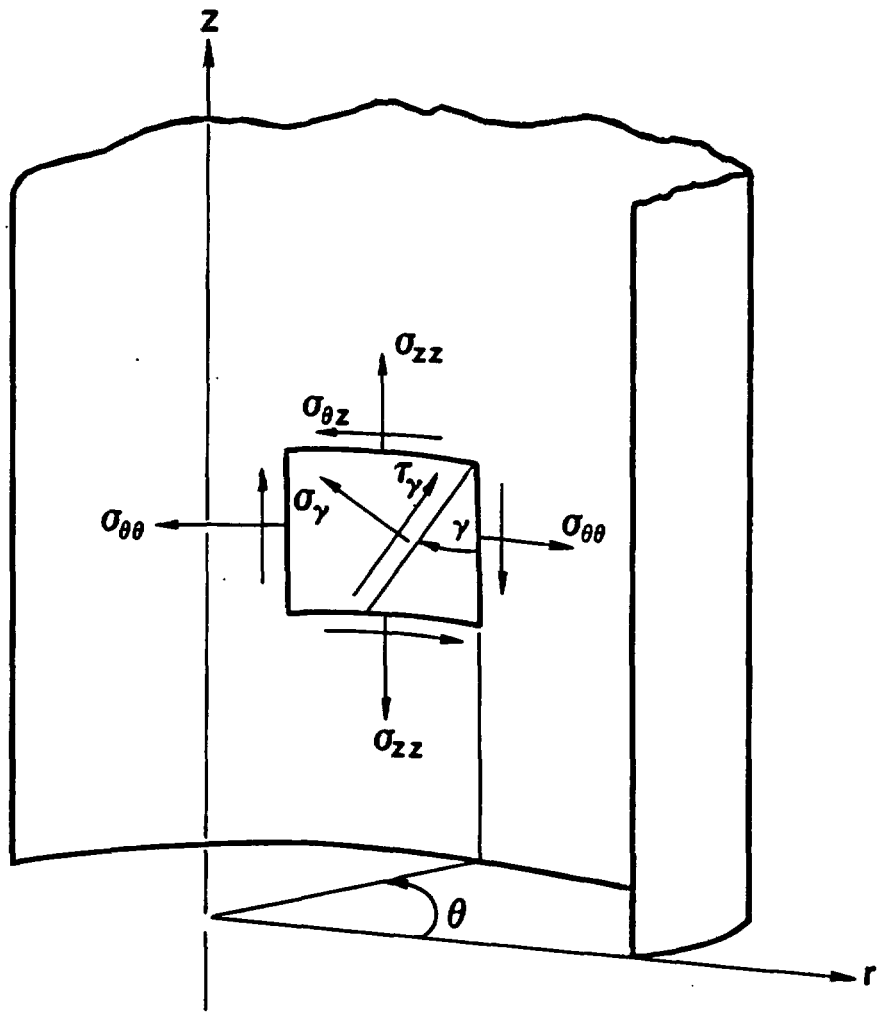

Figure B1. Stress System at Borehole Surface

References

[B1] A. E. H. Love, A Treatise on the Mathematical Theory of Elasticity (4th ed; NY: Dover Publications, n.d.), p. 90. First American Printing, 1944.

[B2] E. R. Leeman, "The Determination of the Complete State of Stress in Rock in a Single Borehole--Laboratory and Underground Measurements," Int J Rock Mech Min Sci, 5:31-56 (1968).

APPENDIX C

Uniform Stress Field Referred to Principal Stresses

This appendix considers the stresses on an element of material rotated from the principal stress directions to the directions of the coordinates of the cylindrical cavity. The general Euler angles shown in Figure C1 are used.

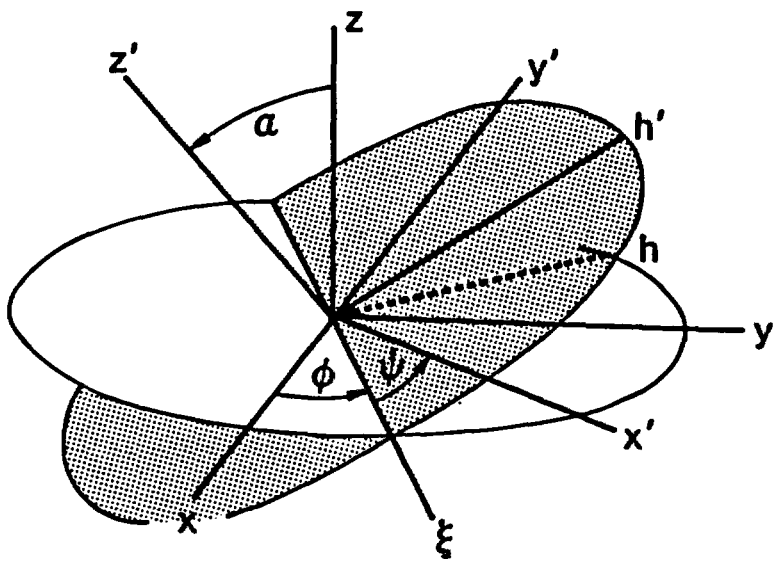

Figure C1. General Euler Angles

The transformation which takes $(x,y,z) = \underset{\sim}{X}$ into $(x',y',z') = \underset{\sim}{X}'$ is

$$\underset{\sim}{X}' = A\,\underset{\sim}{X}, \tag{C1}$$

where A is given by Eq. (4-46) in Reference C1 with $\theta \to \alpha$. This gives

$$\begin{aligned}
x' &= (\cos\psi\cos\phi - \cos\alpha\sin\phi\sin\psi)\,x \\
&\quad + (\cos\psi\sin\phi + \cos\alpha\cos\phi\sin\psi)\,y + \sin\psi\sin\alpha\,z \\
y' &= -(\sin\psi\cos\phi + \cos\alpha\sin\phi\cos\psi)\,x \\
&\quad + (-\sin\psi\sin\phi + \cos\alpha\cos\phi\cos\psi)\,y + \cos\psi\sin\alpha\,z \\
z' &= \sin\alpha\sin\phi\,x - \sin\alpha\cos\phi\,y + \cos\alpha\,z
\end{aligned} \tag{C2}$$

The inverse transformation $A^{-1} = A^T$ is immediately obtained as

$$\underset{\sim}{X} = A^T \underset{\sim}{X}' \tag{C3}$$

Now take the $\underset{\sim}{X} = (x,y,z)$ as the coordinates for the principal stresses and transform these principal stresses to the $\underset{\sim}{X}'$ system. The principal stresses will be denoted by σ_{ii}, and the transform stresses in the $\underset{\sim}{X}'$ space will be denoted by $\bar{\sigma}_{ij}$. The transformations provide finally

$$\begin{aligned}
\bar{\sigma}_{xx} &= (\cos\psi\cos\phi - \cos\alpha\sin\phi\sin\psi)^2\,\sigma_{xx} \\
&\quad + (\cos\psi\sin\phi + \cos\alpha\cos\phi\sin\psi)^2\,\sigma_{yy} \\
&\quad + \sin^2\psi\sin^2\alpha\,\sigma_{zz} \\
\bar{\sigma}_{xy} &= -(\cos\psi\cos\phi - \cos\alpha\sin\phi\sin\psi)(\sin\psi\cos\phi + \cos\alpha\sin\phi\cos\psi)\sigma_{xx} \\
&\quad - (\cos\psi\sin\phi + \cos\alpha\cos\phi\sin\psi)(\sin\psi\sin\phi - \cos\alpha\cos\phi\cos\psi)\sigma_{yy} \\
&\quad + \sin\psi\cos\psi\sin^2\alpha\,\sigma_{zz} \\
\bar{\sigma}_{xz} &= \sin\alpha\sin\phi\,(\cos\psi\cos\phi - \cos\alpha\sin\phi\sin\psi)\sigma_{xx} \\
&\quad - \sin\alpha\cos\phi\,(\cos\psi\sin\phi + \cos\alpha\cos\phi\sin\psi)\,\sigma_{yy} \\
&\quad + \sin\alpha\cos\alpha\sin\psi\,\sigma_{zz} \\
\bar{\sigma}_{yy} &= (\sin\psi\cos\phi + \cos\alpha\sin\phi\cos\psi)^2\sigma_{xx} \\
&\quad + (\sin\psi\sin\phi - \cos\alpha\cos\phi\cos\psi)^2\sigma_{yy} \\
&\quad + \cos^2\psi\sin^2\alpha\,\sigma_{zz} \\
\bar{\sigma}_{yz} &= -\sin\alpha\sin\phi\,(\sin\psi\cos\phi + \cos\alpha\sin\phi\cos\psi)\sigma_{xx} \\
&\quad + \sin\alpha\cos\phi\,(\sin\psi\sin\phi - \cos\alpha\cos\phi\cos\psi)\sigma_{yy} \\
&\quad + \sin\alpha\cos\alpha\cos\psi\,\sigma_{zz} \\
\bar{\sigma}_{zz} &= \sin^2\alpha\sin^2\phi\,\sigma_{xx} + \sin^2\alpha\cos^2\phi\,\sigma_{yy} + \cos^2\alpha\,\sigma_{zz}\,.
\end{aligned} \tag{C4}$$

The $\bar{\sigma}_{ij}$ stresses of Eq. (C4) are the uniform stresses in the (x',y',z') coordinate system of Figure C1 and are the stresses to be used in the analysis of Appendix B where z' is the axis of the cylindrical borehole. This provides the borehole stresses in terms of the three principal stresses in (x,y,z) and the three directions defined by the Euler angles.

The inverse transform gives

$$\sigma_{xx} = (\cos\psi\cos\phi - \cos\alpha\sin\phi\sin\psi)^2\sigma_{xx}'$$

$$+ (\sin\psi\cos\phi + \cos\alpha\sin\phi\cos\psi)^2\sigma_{yy}'$$

$$+ \sin^2\alpha\sin^2\phi\,\sigma_{zz}'$$

$$\sigma_{xy} = (\cos\psi\cos\phi - \cos\alpha\sin\phi\sin\psi)(\cos\psi\sin\phi + \cos\alpha\cos\phi\sin\psi)\sigma_{xx}'$$

$$+ (\sin\psi\cos\phi + \cos\alpha\sin\phi\cos\psi)(\sin\psi\sin\phi - \cos\alpha\cos\phi\cos\psi)\sigma_{yy}'$$

$$- \sin^2\alpha\sin\phi\cos\phi\,\sigma_{zz}'$$

$$\sigma_{xz} = \sin\alpha\sin\psi\,(\cos\psi\cos\phi - \cos\alpha\sin\phi\sin\psi)\sigma_{xx}'$$

$$- \sin\alpha\cos\psi\,(\sin\psi\cos\phi + \cos\alpha\sin\phi\cos\psi)\sigma_{yy}'$$

$$+ \sin\alpha\cos\alpha\sin\phi\,\sigma_{zz}'$$

$$\sigma_{yy} = (\cos\psi\sin\phi + \cos\alpha\cos\phi\sin\psi)^2\sigma_{xx}'$$

$$+ (\sin\psi\sin\phi - \cos\alpha\cos\phi\cos\psi)^2\sigma_{yy}'$$

$$+ \sin^2\alpha\cos^2\phi\,\sigma_{zz}'$$

$$\sigma_{yz} = \sin\alpha\sin\psi\,(\cos\psi\sin\phi + \cos\alpha\cos\phi\sin\psi)\sigma_{xx}'$$

$$- \sin\alpha\cos\psi\,(\sin\psi\sin\phi - \cos\alpha\cos\phi\cos\psi)\sigma_{yy}'$$

$$- \cos\alpha\sin\alpha\cos\phi\,\sigma_{zz}'$$

$$\sigma_{zz} = \sin^2\alpha\sin^2\psi\,\sigma_{xx}' + \sin^2\alpha\cos^2\psi\,\sigma_{yy}' + \cos^2\alpha\,\sigma_{zz}' \quad \text{(C5)}$$

where σ_{xx}', σ_{yy}', σ_{zz}' are principal stresses referred to the X' coordinates.

The σ_{ij} stresses of Eq. (C5) are the uniform stresses in the (x,y,z) coordinate system of Figure C1 and can also be used in the analysis of Appendix B where z is now the axis of the cylindrical borehole. In a particular application, some information about the magnitude of the principal stress and directions may be available, and it may be more convenient to use one or the other of Eqs. (C4) and (C5), depending on what angles or stresses are known. Either one provides the borehole stresses of Appendix B in terms of the three principal stresses and the Euler angles.

Note that the last rotation in A, that is, the ψ rotation, is simply a rotation about the cylindrical axis z' and can be designated as a θ_o in the (r,θ,z) coordinates. Taking $\psi = 0$, the transformed stresses of Eq. (C4) become

$$\bar{\sigma}_{xx} = \cos^2 \phi\, \sigma_{xx} + \sin^2 \phi\, \sigma_{yy}$$

$$\bar{\sigma}_{xy} = - \cos \alpha \cos \phi \sin \phi\, (\sigma_{xx} - \sigma_{yy})$$

$$\bar{\sigma}_{xz} = \sin \alpha \cos \phi \sin \phi\, (\sigma_{xx} - \sigma_{yy})$$

$$\bar{\sigma}_{yy} = \cos^2 \alpha \sin^2 \phi\, \sigma_{xx} + \cos^2 \alpha \cos^2 \phi\, \sigma_{yy} + \sin^2 \alpha\, \sigma_{zz}$$

$$\bar{\sigma}_{yz} = - \sin \alpha \cos \alpha\, [\sin^2 \phi\, \sigma_{xx} + \cos^2 \phi\, \sigma_{yy} - \sigma_{zz}]$$

$$\bar{\sigma}_{zz} = \sin^2 \alpha \sin^2 \phi\, \sigma_{xx} + \sin^2 \alpha \cos^2 \phi\, \sigma_{yy} + \cos^2 \alpha\, \sigma_{zz} \,. \qquad \text{(C6)}$$

While Eq. (C6) is somewhat simpler in form than (C4), the angle θ_o in the cylindral coordinate system is still unknown, so no more information is available.

It is often useful to rotate the coordinate system about the cylindrical borehole axis z or z'. Transformed stresses due to this rotation are recorded here. Neither the original nor the rotated coordinate system is assumed to be oriented along the principal stress directions. The transformation from $\underset{\sim}{X}$ to $\underset{\sim}{X}''$ for a rotation about the z-axis through an angle θ is given by $\underset{\sim}{X}'' = D\underset{\sim}{X}$, where

$$D = \begin{bmatrix} \cos\theta & \sin\theta & 0 \\ -\sin\theta & \cos\theta & 0 \\ 0 & 0 & 1 \end{bmatrix} , \qquad \text{(C7)}$$

and the stresses σ_{ij}'' in $\underset{\sim}{X}''$ in terms of the stresses σ_{ij} in $\underset{\sim}{X}$ are given by

$$\sigma_{xx}'' = \cos^2 \theta\, \sigma_{xx} + \sin^2 \theta\, \sigma_{yy} + 2 \cos \theta \sin \theta\, \sigma_{xy}$$

$$\sigma_{xy}'' = - \cos \theta \sin \theta\, (\sigma_{xx} - \sigma_{yy}) + (\cos^2 \theta - \sin^2 \theta)\sigma_{xy}$$

$$\sigma_{xz}'' = \cos \theta\, \sigma_{xz} + \sin \theta\, \sigma_{yz}$$

$$\sigma_{yy}'' = \sin^2 \theta\, \sigma_{xx} + \cos^2 \theta\, \sigma_{yy} - 2 \sin \theta \cos \theta\, \sigma_{xy}$$

$$\sigma_{yz}'' = - \sin \theta\, \sigma_{xz} + \cos \theta\, \sigma_{yz}$$

$$\sigma_{zz}'' = \sigma_{zz} \,. \qquad \text{(C8)}$$

Reference

[C1] H. Goldstein, Classical Mechanics (Cambridge, MA: Addison-Wesley Publishing Co, 1956), Ch 4.

APPENDIX D

Overburden Stress under an Inclined Geologic Surface

In this appendix, several possible states of stress arising from the overburden of an inclined geologic surface are considered. Classical linear elasticity is used with a positive normal stress defining a tensile stress, and a simple change of sign of the stress tensor then provides the results needed in the body of this report. The geologic formation is assumed to be an isotropic, homogeneous, linearly-elastic half plane under conditions of plane strain and subjected to a vertical gravitational body force (ρg), where ρ is the rock density and g is the gravitational acceleration. The surface of the half plane is inclined at an angle α from the horizontal x-axis, measured as shown in Figure D1.

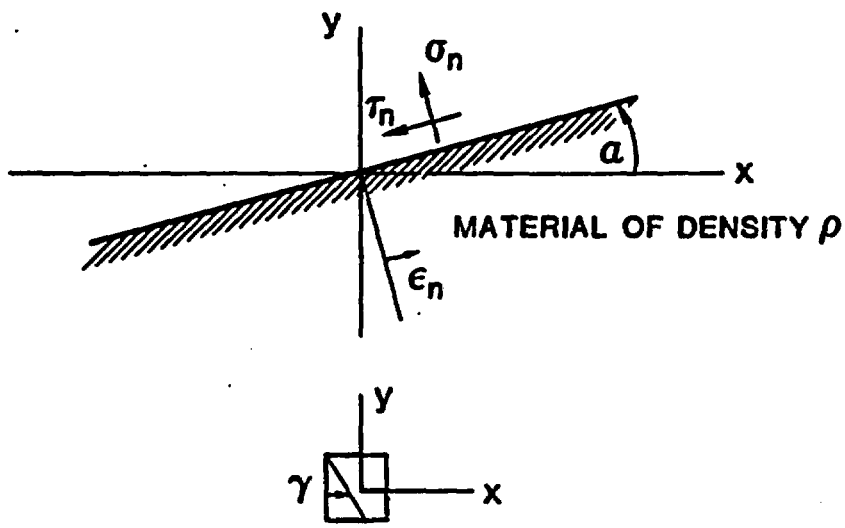

Figure D1. Cross-Sectional Diagram of Inclined Geological Formation

From the polynomial solutions for a body force,[D1]

$$\sigma_x = c_3\, x + d_3\, y$$

$$\sigma_y = a_3\, x + b_3\, y + \rho g\, y$$

$$\tau_{xy} = -b_3\, x - c_3\, y$$

$$\sigma_z = \nu\,(\sigma_x + \sigma_y)\ , \qquad \text{(D1)}$$

and

$$\epsilon_x = \frac{(1+\nu)}{E}\,[(1-\nu)\,\sigma_x - \nu\,\sigma_y]$$

$$\epsilon_y = \frac{(1 + \nu)}{E} [(1 - \nu) \sigma_y - \nu \sigma_x]$$

$$\gamma_{xy} = \frac{2(1 + \nu)}{E} \tau_{xy} , \tag{D2}$$

where E, ν are the formation elastic modules and Poisson's ratio, respectively,[D1] the normal stress on the plane inclined at angle α, as shown in Figure D1, is

$$\sigma_n = [c_3 x + d_3 y] \sin^2 \alpha + [a_3 x + (b_3 + \rho g) y] \cos^2 \alpha$$

$$+ 2 [b_3 x + c_3 y] \sin \alpha \cos \alpha , \tag{D3}$$

and the shear stress is given by

$$\tau_n = [(c_3 - a_3) x + (d_3 - b_3 - \rho g) y] \sin \alpha \cos \alpha$$

$$+ (b_3 x + c_3 y)(\cos^2 \alpha - \sin^2 \alpha) . \tag{D4}$$

Now, regardless of what other conditions are put on the strains in the material, there must be $\sigma_n = \tau_n = 0$ on the plane

$$y = \tan \alpha \, x . \tag{D5}$$

Substituting Eq. (D5) into Eqs. (D3) and (D4) gives two relations for the coefficients which must be satisfied for all x. These become

$$a_3 \cos^3 \alpha + 3 b_3 \cos^2 \alpha \sin \alpha + 3 c_3 \cos \alpha \sin^2 \alpha$$

$$+ d_3 \sin^3 \alpha = - \rho g \sin \alpha \cos^2 \alpha \tag{D6}$$

$$-a_3 \cos^2 \alpha \sin \alpha + b_3 \cos \alpha (\cos^2 \alpha - 2 \sin^2 \alpha)$$

$$+ c_3 \sin \alpha (2 \cos^2 \alpha - \sin^2 \alpha) + d_3 \cos \alpha \sin^2 \alpha = \rho g \cos \alpha \sin^2 \alpha . \tag{D7}$$

Some possible deformation conditions are now considered.

1. <u>Case 1 -- Uniaxial Vertical Stress</u>

For this case, $\sigma_x = \tau_{xy} = 0$ for all x, y.

Then
$$b_3 = c_3 = d_3 = 0 ,$$
$$a_3 = - \rho g \tan \alpha ,$$

and

$$\sigma_y = \rho g (y - x \tan \alpha) . \tag{D8}$$

This solution represents a direct overburden with no containing stresses in the horizontal direction.

2. Case 2 -- Uniaxial Vertical Strain

For this case, $\epsilon_x = 0$ for all x, y, and Eq. (D2) then provides the two additional equations

$$(1 - \nu)\, c_3 - \nu\, a_3 = 0$$

$$(1 - \nu)\, d_3 - \nu\, (b_3 + \rho g) = 0. \tag{D9}$$

Equations (D6), (D7), and (D9) give

$$a_3 = - K \sin\alpha \cos\alpha$$

$$b_3 = \frac{\nu}{(1 - \nu)} K \sin^2\alpha$$

$$c_3 = - \frac{\nu}{(1 - \nu)} K \sin\alpha \cos\alpha$$

$$d_3 = \frac{\nu}{(1 - \nu)} K \cos^2\alpha \ ,$$

where

$$K = \frac{\rho g}{[\cos^2\alpha - \frac{\nu}{(1 - \nu)} \sin^2\alpha]} \ ,$$

and the stresses become

$$\sigma_x = \sigma_z = - \frac{\rho g \nu}{(1-\nu)} \frac{\cos\alpha\ (\sin\alpha\ x - \cos\alpha\ y)}{[\cos^2\alpha - \frac{\nu}{(1 - \nu)} \sin^2\alpha]}$$

$$\sigma_y = - \frac{\rho g \cos\alpha\ (\sin\alpha\ x - \cos\alpha\ y)}{[\cos^2\alpha - \frac{\nu}{(1 - \nu)} \sin^2\alpha]} \tag{D10}$$

$$\tau_{xy} = - \frac{\rho g \nu}{(1 - \nu)} \frac{\sin\alpha\ (\sin\alpha\ x - \cos\alpha\ y)}{[\cos^2\alpha - \frac{\nu}{(1 - \nu)} \sin^2\alpha]} \ .$$

The maximum and minimum principal stresses are

$$\sigma_{\substack{min \\ max}} = - \frac{\rho g}{2(1 - \nu)} \frac{(\sin\alpha\ x - \cos\alpha\ y) \cos\alpha}{[\cos^2\alpha - \frac{\nu}{(1 - \nu)} \sin^2\alpha]} \times$$

$$\left\{1 \pm \sqrt{(1 - 2\nu)^2 + 4\nu^2 \operatorname{Tan}^2\alpha}\ \right\} , \tag{D11}$$

and these will occur on planes at an angle γ from the vertical given by

$$\tan 2\gamma = - \frac{2\nu}{(1 - 2\nu)} \tan\alpha \ . \tag{D12}$$

The angle γ is shown on an element of material in Figure D1. This is an interesting result in the sense that the angle γ is constant throughout the material. In particular, the free surface of the material is <u>not</u> a principal stress direction.

The significance of the angle $\alpha = \alpha_o$, such that $\cos^2 \alpha_o = (\nu/(1 - \nu)) \sin^2 \alpha_o$, is not obvious.

3. Case 3 -- Uniaxial Strain Normal to Inclined Surface

For this case, $\varepsilon_n = 0$ for all x, y and Eq. (D2) provides

$$\varepsilon_n = \frac{(1 + \nu)}{2E} \left\{(1 - 2\nu)(\sigma_x + \sigma_y) + (\sigma_x - \sigma_y) \cos 2\alpha + 2\ \tau_{xy} \sin 2\alpha\right\} = 0 \ . \quad \text{(D13)}$$

Substitution from (D1) gives the two equations

$$(1 - 2\nu)(c_3 + a_3) + (c_3 - a_3)(\cos^2 \alpha - \sin^2 \alpha) - 4\ b_3 \sin \alpha \cos \alpha = 0 \quad \text{(D14)}$$

$$(1 - 2\nu)(d_3 + b_3 + \rho g) + (d_3 - b_3 - \rho g)(\cos^2 \alpha - \sin^2 \alpha)$$

$$- 4\ c_3 \sin \alpha \cos \alpha = 0 \quad \text{(D15)}$$

Solving Eqs. (D6), (D7), (D14), and (D15) gives

$$a_3 = \frac{\rho g}{(1 - \nu)} \sin \alpha \cos \alpha\ [\cos^2 \alpha - (2 - \nu)]$$

$$b_3 = - \frac{\rho g}{(1 - \nu)} \sin^2 \alpha\ (\sin^2 \alpha - \nu)$$

$$c_3 = \frac{\rho g}{(1 - \nu)} \sin \alpha \cos \alpha\ (\sin^2 \alpha - \nu)$$

$$d_3 = - \frac{\rho g}{(1 - \nu)} \cos^2 \alpha\ (\sin^2 \alpha - \nu) \ .$$

The stresses, from Eq. (D1), become

$$\sigma_x = \frac{\rho g}{(1 - \nu)} \cos \alpha\ (\sin^2 \alpha - \nu)(\sin \alpha\ x - \cos \alpha\ y)$$

$$\sigma_y = - \frac{\rho g}{(1 - \nu)} \cos \alpha\ [\sin^2 \alpha + (1 - \nu)]\ (\sin \alpha\ x - \cos \alpha\ y)$$

$$\tau_{xy} = \frac{\rho g}{(1 - \nu)} \sin \alpha\ (\sin^2 \alpha - \nu)(\sin \alpha\ x - \cos \alpha\ y)$$

$$\sigma_z = - \frac{\nu \rho g}{(1 - \nu)} \cos \alpha\ (\sin \alpha\ x - \cos \alpha\ y) \quad \text{(D16)}$$

The maximum principal stresses are

$$\sigma_{\substack{min \\ max}} = - \frac{\rho g}{2(1 - \nu)} \left[\cos \alpha \pm \sqrt{(1 - 2\nu)^2 + (3 - 4\nu) \sin^2 \alpha}\right]$$

$$x(\sin \alpha\ x - \cos \alpha\ y) \ , \quad \text{(D17)}$$

and these occur at an angle γ such that

$$\text{Tan } 2\gamma = \frac{2\,(\sin^2 \alpha - \nu)\,\tan \alpha}{[2 \sin^2 \alpha + (1 - 2\nu)]} \,. \tag{D18}$$

As in Case 2, the angle γ is constant throughout the material, and the free surface is not a principal stress direction.

Other material restraints could be considered, but the three cases discussed would appear to be the most logical. Of these, Case 2, which restricts the deformation to uniaxial vertical strain, seems most realistic and predicts a maximum principal stress and fracture plane inclined from the vertical through the angle γ in the direction of the terrain gradient. This general effect has been observed through minebacking in G Tunnel although the angle of inclination is greater than predicted by Eq. (D12). This is to be expected since other in-situ effects in addition to overburden are operating here. For level terrain, for example, with $\alpha = 0$, Eq. (D10) provides $\sigma_x = \sigma_z = \frac{\nu}{(1-\nu)}\,\sigma_y$, which is the classical uniaxial vertical strain overburden which is not verified by experimental results.

Reference

[D1] S. Timoshenko and J. N. Goodier, Theory of Elasticity, 2nd ed (New York: McGraw-Hill Inc, 1951), p 30.

DISTRIBUTION:

Lawrence Livermore National Lab (9)
P.O. Box 808
Livermore, CA 94550
Attn: J. N. Shearer, L-51
R. C. Carlson, L-204
B. C. Hudson, L-48
H. O. Glenn, L-200
R. W. Terhune, L-200
G. H. Higgins, L-209
H. L. McKague, L-222
F. E. Heuzel, L-350
D. F. Towse, L-224

Los Alamos National Lab (4)
P.O. Box 1663
Los Alamos, NM 87545
Attn: E. M. Jones, MS-665
F. N. App, MS-665
R. R. Brownlee, MS-570
P. L. Aamodt, MS-595

DOE/DNA
FCTC
P.O. Box 208
Mercury, NV 89023
Attn: J. W. LaComb

Defense Nuclear Agency (2)
Kirtland Air Force Base
Albuquerque, NM 87115
Attn: C. E. Keller, FCTMC
B. Ristvet, FCTMC

USGS--Denver Federal Center (3)
P.O. Box 25046
Denver, CO 80225
Attn: W. S. Twenhofel, MS-954
W. Ellis, MS-954
R. D. Carroll, MS-954

Systems, Science & Software
P.O. Box 1620
La Jolla, CA 92037
Attn: R. E. Duff

Fenix & Scisson, Inc.
MS: 940
Mercury, NV 89023
Attn: M. J. O'Brien

Pacifica Technology (2)
P.O. Box 148
Del Mar, CA 92014
Attn: J. Kent
D. Patch

R&D Associates (3)
P.O. Box 9695
Marina del Rey, CA 90291
Attn: J. Lewis
J. Whitner
G. Rawson

Terra Tek, Inc. (7)
420 Wakara
Salt Lake City, UT 84108
Attn: S. Butters
M. D. Voegele
A. H. Jones
J. M Gronseth
A. Abou-Sayed
C. E. Brechtel
S. Green

ARCO Oil and Gas Company (2)
P.O. Box 2819
Dallas, TX 75221
Attn: B. H. Addams
F. G. Martin

ARCO Exploration & Production Research
P. O. Box 2819
Dallas, TX 75221
Attn: M. L. Batzle

Amoco Production Company (5)
Research Center
P.O. Box 591
Tulsa, OK 74102
Attn: F. O. Jones
R. A. Nelson
K. G. Nolte
M. B. Smith
R. W. Veatch, Jr.

Exxon Production Research Company (3)
P.O. Box 2189
Houston, TX 77001
Attn: D. H. Johnston
T. Koelsch
D. M. Kehn

Conoco, Inc. (2)
P.O. Box 2197
Houston, TX 77001
Attn: M. W. Osborne
H. O. McLeod

Chevron Oil Field Research Co. (2)
P.O. Box 446
La Habra, CA 90631
Attn: J. C. Martin
A. Timur

Cities Service Company (2)
P.O. Box 50408
Tulsa, OK 74150
Attn: L. P. Brown
W. Rizer

Mobil R&D Corporation (4)
P.O. Box 900
Dallas, TX 75221
Attn: N. Stein
D. M. Summers
W. L. Medlin
N. R. Goins
J. H. Halsey

Halliburton Services
Research Center
Drawer 1431
Duncan, OK 73533
Attn: A. A. Daneshy

Phillips Petroleum Company, R&D
314 TRW
Bartlesville, OK 74003
Attn: R. E. Hoard

Columbia Gas Systems Service
1600 Dublin Road
Columbus, OH 43215
Attn: S. F. McKetta

Gulf Science & Technology (2)
P.O. Drawer 2038
Pittsburgh, PA 15230
Attn: D. W. Baker
W. Narr

Shell Oil Company
P.O. Box 831
Houston, TX 77001
Attn: J. T. Smith

Shell Development Company (4)
P.O. Box 481
Houston, TX 77001
Attn: W. R. Purcell
M. Pratts
K. S. Hansen
R. J. Saucier

Shell Research
Shell Mex. House
Steamer, London
WC2R ODX
United Kingdom
Attn: J. Geertsma

Union Oil Company of California
P.O. Box 76
Brea, CA 92621
Attn: D. Outmans

Department of Mechanical Engineering (2)
Massachusetts Institute of Technology
Cambridge, MA 02139
Attn: W. F. Brace
M. P. Cleary

USGS (2)
Reston, VA 22092
Attn: M. Zoback
J. D. Bredehoeft

Dowell Division of Dow Chemical
P.O. Box 21
Tulsa, OK 74102
Attn: N-K Ren

Lamont-Doherty Geological
Observatory (3)
Palisades, NY 10964
Attn: R. A. Plumb
Y. P. Aggarwal
T. Engelder

USGS
345 Middlefield Road
Menlo Park, CA 94025
Attn: A. McGarr

Brown University
Division of Engineering
Providence, RI 02912
Attn: R. J. Clifton

University of Wisconsin (3)
1509 University Avenue
Madison, WI 53706
Attn: R. de la Cruz
B. C. Haimsen
H. Pincus

Department of Civil Engineering (2)
University of California
Berkeley, CA 94720
Attn: R. Nolting
R. E. Goodman

Lawrence Berkeley Laboratory
1 Cyclotron Road
Berkeley, CA 94720
Attn: T. Dow

Department of Mechanical Engineering
Rice University
P.O. Box 1892
Houston, TX 77001
Attn: J. B. Cheatham, Jr.

Center for Tectonophysics (3)
Texas A&M University
College Station, TX 77843
Attn: M. Friedman
J. M. Logan
E. R. Hoskins

University of Texas
Department of Petroleum Engineering
Austin, TX 78712
Attn: K. Gray

Stanford University
Palo Alto, CA 94305
Attn: A. Nur

Science Applications, Inc. (2)
Suite, Chestnut Ridge Prof. Bldg.
Morgantown, WV
Attn: J. Pasini, III
L. Z. Shuck

Dames & Moore
"The Limes"
123 Mortlake High St.
London, SW14 8SN, England
Attn: T. R. Harper

Paslay Associates
7417 Brompton Blvd.
Houston, TX 77025
Attn: P. Paslay

University of Arizona
Department of Geosciences
Tucson, AZ 85721
Attn: R. M. Richardson

Lynes, Inc.
P.O. Box 12486
Houston, TX 77017
Attn: C. McClain

1000	G. A. Fowler
1100	C. D. Broyles
1110	J. D. Plimpton
1111	R. C. Bass
1112	C. R. Mehl
1112	C. W. Smith (10)
1116	C. W. Cook
1116	R. P. Reed
1130	H. E. Viney
1131	B. G. Edwards
1131	R. J. Dye (3)
1131	J. S. Talbutt
1133	R. D. Statler
1133	W. C. Vollendorf (10)
1133	C. W. Gulick
4537	L. D. Tyler
4747	R. R. Boade
4752	R. A. Schmidt
4753	S. J. Finley
4753	D. A. Northrop
4753	N. R. Warpinski
4753	J. A. Clark
4754	C. L. Schuster
5531	W. E. Warren (10)
5532	L. W. Teufel
5534	D. E. Grady
8214	M. A. Pound
3141	L. J. Erickson (5)
3151	W. L. Garner (3) For DOE/TIC (Unlimited Release)
3154-3	J. Hernandez (25) For DOE/TIC

☆U.S. GOVERNMENT PRINTING OFFICE: 1981-0-777-023/565

Org.	Bldg.	Name	Rec'd by	Org.	Bldg.	Name	Rec'd by